Molecular Psychiatry (2021) 26:2943–2963
https://doi.org/10.1038/s41380-020-00863-8

ARTICLE

TrkB receptor cleavage by delta-secretase abolishes its phosphorylation of APP, aggravating Alzheimer's disease pathologies

Yiyuan Xia[1,2] · Zhi-Hao Wang[1] · Pai Liu[1,3] · Laura Edgington-Mitchell[4] · Xia Liu[1] · Xiao-Chuan Wang[2,5] · Keqiang Ye[1]

Received: 24 March 2020 / Revised: 27 July 2020 / Accepted: 30 July 2020 / Published online: 11 August 2020

Abstract

Neurotrophins promote neuronal survival and synaptic plasticity via activating the tropomyosin receptor kinases. BDNF and its high-affinity receptor TrkB are reduced in Alzheimer's disease (AD), contributing to progressive cognitive decline. However, how the signaling mediates AD pathologies remains incompletely understood. Here we show that the TrkB receptor binds and phosphorylates APP, reducing amyloid-β production, which are abrogated by δ-secretase cleavage of TrkB in AD. Remarkably, BDNF stimulates TrkB to phosphorylate APP Y687 residue that accumulates APP in the TGN (Trans-Golgi Network) and diminishes its amyloidogenic cleavage. Delta-secretase cleaves TrkB at N365 and N486/489 residues and abolishes its neurotrophic activity, decreasing p-APP Y687 and altering its subcellular trafficking. Notably, both TrkB and APP are robustly cleaved by δ-secretase in AD brains, accompanied by mitigated TrkB signaling and reduced p-Y687. Blockade of TrkB cleavage attenuates AD pathologies in 5xFAD mice, rescuing the learning and memory. Viral expression of TrkB 1-486 fragment in the hippocampus of APP/PS1 mice facilitates amyloid pathology and mitigates cognitive functions. Hence, δ-secretase cleaves TrkB and blunts its phosphorylation of APP, facilitating AD pathogenesis.

Introduction

Neurotrophins including NGF, BDNF, NT3, and NT4/5 support neural development, synaptic plasticity, maintenance of the adult nervous system and learning and memory. The major receptors for these neurotrophic factors include tropomysin-related kinase (Trk) receptors type A, type B, and type C (TrkA, TrkB, and TrkC) and p75NTR. Pro-neurotrophins bind to p75NTR/sortilin preferably, triggering death signaling in cells, while mature neurotrophins interact with Trk receptors predominantly, promoting cell growth and survival [1]. Alzheimer's disease (AD) is the most common neurodegenerative disease with dementia, the principal clinical manifestation during ageing. The pathological features of AD are senile plaques, mainly consisted of extracellular amyloid-β (Aβ) accumulation, and intraneuronal neurofibrillary tangles (NFT), predominantly composed of hyperphosphorylated and truncated microtubule-associated protein Tau. Aβ is generated from sequential proteolytic cleavage of APP by BACE1 (β-secretase) and γ-secretase [2]. Neurotrophic factors deregulation plays an important role in AD disease progression [3]. For instance, mature NGF levels decreased

These authors contributed equally: Yiyuan Xia, Zhi-Hao Wang

Supplementary information The online version of this article (https://doi.org/10.1038/s41380-020-00863-8) contains supplementary material, which is available to authorized users.

✉ Xiao-Chuan Wang
wxch@mails.tjmu.edu.cn

✉ Keqiang Ye
kye@emory.edu

[1] Department of Pathology and Laboratory Medicine, Emory University School of Medicine, Atlanta, GA 30322, USA

[2] Department of Pathophysiology, Key Laboratory of Ministry of Education of Neurological Diseases, Tongji Medical College, Huazhong University of Science and Technology, Wuhan, China

[3] Neuroscience Program, Laney Graduate School, Emory University School of Medicine, Atlanta, GA, USA

[4] Department of Biochemistry and Molecular Biology, School of Biomedical Sciences, The University of Melbourne, Melbourne, VIC 3010, Australia

[5] Co-innovation Center of Neuroregeneration, Nantong University, Nantong, Jiangsu 226001, China

significantly in the basal forebrain of aged animals and AD patients, causing reduction of nerve fibers density, cell atrophy, and down-regulation of transmitter-associated enzymes such as choline acetyltransferase and acetylcholinesterase, thus a decrease of cholinergic transmission [4]; by contrast, the levels of proNGF (precursor of NGF) are elevated in frontal, occipital cortex and hippocampus in late-stage of AD [5, 6] and increased 40–50% in individuals with mild cognitive impairment (MCI) [7], suggesting that an unbalance in NGF processing may contribute to the onset of AD. In addition to NGF/TrkA, BDNF/TrkB signaling also plays important roles in amyloidogenic processing. For example, BDNF level is decreased in AD patient brains [8–10]. BDNF represses Aβ generation in primary neuronal cultures [11], which is elevated by BDNF deprivation [12]. Notably, neurons tolerating NFTs stop BDNF expression, whereas neurons with high levels of BDNF escape from tangles [13]. Therefore, BDNF possesses a protective role against AD pathogenesis. Accordingly, BDNF administration increases learning and memory in impaired animals [14], and BDNF displays a prominent neuroprotective effect against β-amyloid toxicity in AD models. Thus, BDNF gene delivery has thus been proposed as a potential novel therapeutic in AD [15, 16]. Most recently, we show that BDNF/TrkB deficiency stimulates δ-secretase activation via upregulating C/EBPβ in AD [17, 18]. BDNF reduction elicits δ-secretase cleavage of Tau N368, which tightly associates with TrkB receptor and antagonizes its neurotrophic activities [19]. Consequently, a small TrkB agonist 7,8-dihydroxoflavone (7,8-DHF) or its prodrug R13, strongly activates TrkB signaling and displays promising therapeutic efficacy toward AD [20–22].

Delta-secretase is an asparagine endopeptidase (AEP, gene name legumain, *LGMN*) that distributes in the endolysosomes. We have shown that it is activated under stroke or ischemia and cuts SET, a nuclear DNase inhibitor, triggering neuronal cell death [23]. Furthermore, we reported that δ-secretase cleaves APP extracellular domain at N373 and N585 residues and facilitates BACE1 to swiftly cut the substrate APP 586-695 (following the numbering of brain APP 695 isoform), promoting Aβ production [24]. Moreover, δ-secretase shreds Tau at N368 and promotes its aggregation, accelerating neurodegeneration in AD [25]. Interestingly, we also found that BDNF/TrkB pathway activates Akt, which phosphorylates δ-secretase on T322 residue, inhibiting its activation [26]. In the current study, we report that δ-secretase cleaves TrkB receptor on N365 and N486/489 residues located in the extracellular and intracellular domain (ICD), respectively, blocking BDNF neurotrophic signalings. Remarkably, TrkB binds APP and BDNF enhances APP Y687 phosphorylation by TrkB, which elicits p-APP TGN (trans-Golgi-network) translocation and diminishes its proteolytic cleavage by δ-secretase, resulting in Aβ reduction. Consequently, overexpression of δ-secretase-uncleavable TrkB N486/489 A in the hippocampus of 5xFAD mice attenuates AD pathologies and mitigates cognitive dysfunctions. Conversely, viral expression of δ-secretase-truncated TrkB fragment (1-486) in APP/PS1 mice blunts BDNF signalings and facilitates amyloid pathologies, exacerbating cognitive impairment. Therefore, δ-secretase cleaves both TrkB and APP and accelerates AD pathogenesis.

Materials and methods

Cell culture, Mice, and human tissue samples

HEK293 cells (From ATCC) were cultured in medium containing DMEM (high-glucose), 10% fetal bovine serum (FBS), penicillin (100 units/ml)-streptomycin (100 μg/ml) (all from Hyclone). SH-SY5Y cells (From ATCC) were cultured in medium containing RPMI 1640, 10% FBS and penicillin (100 units/ml)-streptomycin (100 μg/ml). Integrin beta1 subunit was validated in HEK293 cell line. Cells were incubated at 37 °C in a humidified atmosphere of 5% CO_2. Primary rat cortical neurons were cultured as previously reported [25]. All rats were bought from the Jackson Laboratory. The protocol was reviewed and approved by the Emory Institutional Animal Care and Use Committee. 5XFAD mice and APP/PS1 mice were obtained from the Jackson Laboratory (Stock No. 006554 and 004462, respectively). AEP knockout mice were generated as previously described [25]. The following animal groups were analyzed: WT, APP/PS1, 5XFAD, $AEP^{-/-}$, 5XFAD/$AEP^{-/-}$. The animals were assigned to different experimental groups based on the litter and gender in a way that every experimental group had similar number of siblings' males and females. Animal care and handling were performed according to the Declaration of Helsinki and Emory Medical School guidelines. Postmortem brain samples were dissected from frozen brains of 4 AD cases and 4 non-demented controls from the Emory Alzheimer's Disease Research Center (Table S1). All procedures performed in studies involving human participants were in accordance with the ethical standards of the institutional and/or national research committee and with the 1964 Helsinki declaration and its later amendments or comparable ethical standards. AD was diagnosed according to the criteria of the Consortium to Establish a Registry for AD and the National Institute of Aging. Diagnoses were confirmed by the presence of amyloid plaques and NFT in formalin-fixed tissue. Informed consent was obtained from the subjects. The study was approved by the Biospecimen Committee.

Transfection and infection of the cells

The overexpressing plasmids and siRNAs were ordered from Addgene and Santa Cruz respectively. The overexpression lentivirus (pFCGW-GFP vector) were packaged from the viral vector core of Emory University, which were used in neurons and mice. Lipofectamine 3000 (Invitrogen) was used for HEK293 and SH-SY5Y cells transfection.

Differentiation of human iPSC-derived NSCs into neurons

We used Human iPSC-derived NSCs obtained from 2 donors: ACS-5003 from normal human, ATCC (Manassas, US), ax0111 from AD patient with ApoE4/4 genotype, Axol Bioscience (Cambridge, UK). Neuron differentiation from NSCs was accomplished by culturing on PLO/Laminin-coated plates in neuronal differentiation medium, which contains DMEM/F12 + Neurobasal Medium (1: 1), GDNF (20 ng/ml), supplemented with BDNF, B27, N2(20 ng/ml), IGF (10 ng/ml), NT3 (10 ng/ml), ascorbic acid (200 μM) (all from Stemcell Technologies) and dbcAMP (100 nM) (Sigma Aldrich). In 48 h, neuronal culture medium was changed to remove unattached cells, then medium were be half changed every 3 days during in vitro maturation.

TrkB in vitro kinase assay

Human recombinant YFP-TrkB WT and TrkB KD plasmids were transfected into SH-SY5Y cells and pretreated with/without K252a (100 nM) for 15 min, followed with/without BDNF (50 ng/ml) for 30 min. After 48 h, the TrkB proteins were purified by immunoprecipitation (IP). With the prediction of kinase-specific phosphorylation sites system, peptide ^{683}ENPTYKFFEQ^{692} (Peptide Y^{687}) and ^{683}ENPTFKFFEQ^{692} (Peptide F^{687}) were synthesized from Peptide 2.0 Inc. USA, TrkB Kinase Buffer: 40 mM Tris, pH 7.5; 0.1 mg/ml BSA; 2.5 mM $MnCl_2$; 20 mM $MgCl_2$; 50 μM DTT, containing freshly prepared 20 μM ATP, and 15 μCi [^{32}P]-ATP (PerkinElmer, #BLU002250UC). Purified TrkB WT or TrkB KD was incubated with [^{32}P]-ATP and peptides for 30 min, then 96-well filter plates with negatively charged phosphor-cellulose were used to wash out the free ^{32}P, and phosphorylated peptides were collected for the protein kinase assays. The results were shown by autoradiography and radiometer.

Generation of antibodies specific for TrkB-phosphorylated APP (anti-APP pY687), TrkB 1-486 (anti-TrkB N486) and TrkB 487-822 (anti-TrkB C487)

Two rabbits received booster injections 4 times with the immunizing peptide (Ac-CENPT (pY)KFFEQ-amide) every 3 weeks intervals. The collected antiserum was purified via affinity chromatography with the immunizing peptide and then was adsorbed to a peptide spanning the phosphorylated site (Ac-CENPTYKFFEQ-amide).

Two rabbits received booster injections 4 times with the immunizing peptide (Ac-CASPLHHISN-OH) every 3 weeks intervals. The collected antiserum was purified via affinity chromatography with the immunizing peptide and then was adsorbed to a peptide spanning the Full length TrkB (Ac-CPLHHISNGSNTPSS-amide).

Two rabbits received booster injections 4 times with the immunizing peptide (H^2N-GSNTPSSSEC-amide) every 3 weeks intervals. The collected antiserum was purified via affinity chromatography with the immunizing peptide and then was adsorbed to a peptide spanning the Full length TrkB (Ac-PLHHISNGSNTPSSC-amide).

AEP activity assay

Cell lysates (10 μg) or tissue homogenates (10 μg) and 20 μM AEP substrate Z-Ala-Ala-Asn-AMC (Bachem) were incubated with 200 μl reaction buffer, which contained 60 mM Na_2HPO_4, 20 mM citric acid, 1 mM EDTA, 1 mM DTT and 0.1% CHAPS, pH 5.5 at 37 °C. Then the AMC released fluorescence by substrate cleavage was measured in a fluorescence plate reader in kinetic mode at 460 nm.

Aβ plaque histology

For immunohistochemical stainning of Aβ, combined with Thioflavin-S staining. Briefly, free-floating 30 μm brain sections were treated with 0.3% H_2O_2 at room temperature for 10 min. After that, sections were washed in PBS with 0.3% Triton X-100 for 3 times, then 1% BSA was used for blocking for 30 min, followed by overnight incubation with anti-Aβ antibody (1: 500, Sigma-Aldrich) at 4 °C. The signal was developed using Histostain-SP kit. After the preparation, the sections were washed in distilled water and stained for 5 min with 0.0125% Thioflavin-S in 50% ethanol. After washing, the sections were covered with a glass cover using mounting solution and took pictures under a fluorescence microscope. The plaque number and plaque area were analyzed using the ImageJ software (National Institutes of Health).

Immunofluorescence

Transfected/treated cells or mice brain slices or human tissues were fixed and incubated overnight at 4 °C with primary antibodies. After washing, the slices were incubated with Alexa Fluor® 568-, 488- or Cy5-conjugated secondary antibodies (Invitrogen) for 1 h at 37 °C. DAPI (Sigma) was used as the nuclei marker. Images were acquired through

Confocal microscope (Olympus FV1000) and analyzed with ImageJ software.

Mass spectrometry analysis

Two 10-cm dishes of HEK293 (~1×10^7 cells each dish) were transfected with 10 μg GST-TrkB plasmids. In 48 h, the transfected cells were collected and lysed in RIPA buffer (20 mM Tris-HCl, pH 7.5, 1 mM EDTA, 1 mM EGTA, 150 mM NaCl, 2.5 mM sodium pyrophosphate, 1% NP-40, 1% sodium deoxycholate, 1 mM Na_3VO_4 and 1 mM β-glycerophosphate) with protease inhibitor cocktail on ice for 20 min. The starting material used for this experiment is 1000 ug. The protein concentration was diluted into 5 μg/μl. Samples were precleared by pre-incubation with protein A/G beads for 20 min in 4 °C, then centrifuged at 14,000 × *g* at 4 °C for 10 min. The supernatants were incubated with Glutathione Sepharose 4B (10 μl) overnight at 4 °C. After washing the beads with pH = 6.0 RIPA buffer for 3 times, then incubated with 1 μg activated AEP (37 kD) at 37 °C for 60 min, shacked every 10 min. The samples were then boiled in 50 μl 1XSDS loading buffer for 10 min and analyzed by Coomassie staining and immunoblotting. Protein samples were in-gel digested with trypsin and analyzed by LC/MS/MS.

Real-time PCR

RNAs from cells and tissues were isolated with Trizol. After reverse transcription with SuperScriptIII reverse transcriptase, Real-time PCR reactions were performed using the ABI 7500-Fast Real-Time PCR System, Gene-specific primers and TaqMan Universal Master Mix Kit were designed and bought from Taqman. All kits and reagents were purchased from Life Technologies. $2^{-\Delta\Delta Ct}$ method was used for the relative quantification of gene expression. For each data point, at least 2 duplicated wells were used.

GST-pull down

The cell lysates were incubated overnight with 20 μl of a 50% slurry of Glutathione Sepharose 4B at 4 °C. Then supernatant was removed after centrifugation at 500 × *g* for 5 min. The Glutathione Sepharose 4B was washed by adding 1 ml lysis buffer to each tube and inverted to mix. Sediment the medium by centrifugation at 500 × *g* for 5 min. After wash for 3 times, the supernatant was decanted carefully, and the sediment was analyzed via Western blot.

Immunoprecipitation and western blotting

The tissues or cells were washed with ice-cold PBS and lysed in RIPA buffer (20 mM Tris-HCl, pH 7.5, 1 mM EDTA, 1 mM EGTA, 150 mM NaCl, 2.5 mM sodium pyrophosphate, 1% NP-40, 1% sodium deoxycholate, 1 mM Na_3VO_4 and 1 mM β-glycerophosphate) with protease inhibitor cocktail for 20 min on ice. The supernatant was collected by centrifuging at 14,000 rpm for 20 min at 4 °C. Then the protein extract was diluted to 5 mg/ml. After electrophoresis, the samples were incubated overnight at 4 °C with primary antibody (antibodies listed in Table S2), followed by immunoblotting.

ELISA quantification of Aβ

The tissues or cells were diluted with cold reaction buffer (PBS, 5% BSA, 0.03% Tween-20, protease inhibitor cocktail), and centrifuged at 16,000 × *g* for 20 min at 4 °C. Then analyzed with human $A\beta_{42}$ (KHB3441, Invitrogen), human $A\beta_{40}$ (KHB3481, Invitrogen), mouse $A\beta_{42}$ (KMB3441, Invitrogen), mouse $A\beta_{40}$ (KMB3481, Invitrogen) ELISA kits.

Subcellular fractionation

Frontal cortex tissue (200 mg) was minced in 1 ml of homogenization buffer (10 mM Tris-HCl, pH 7.4, 0.25 M sucrose, 1 mM $MgCl_2$, protease inhibitor cocktail). After centrifugation at 100 × *g* for 2 min at 4 °C, the supernatant was discarded. The pellet was resuspended in 1.5 ml homogenization buffer and homogenized by successive passages through needles of increasing gauge number. The mixture was centrifuged at 1000 × *g* for 10 min, then supernatant was adjusted to 1.4 M sucrose, and incorporated into a discontinuous sucrose gradient: 2 ml 2 M sucrose, 2.25 ml 1.4 M sucrose, 3.75 ml 1.2 M sucrose and 5 ml 0.8 M sucrose. The gradients were centrifuged at 100,000 × *g* for 2.5 h at 4 °C. After all, 13 fractions were collected from the gradient and stored as aliquots at −80 °C. Equal volumes of fractions were boiled in 1X SDS loading buffer for 10 min and followed by immunoblotting.

Stereotaxic injection in mouse hippocampus

Briefly, animals were anesthetized with isoflurane vaporizer to 2% and given 0.1 mg/kg buprenorphine subcutaneously for pain management. After checked the depth of anesthesia via toe-pinch. The mice heads were shaved and restrained in a stereotaxic frame (Stoeltling, Wood Dale, IL). Sterile erythromycin ophthalmic ointment (0.5%) was applied to the eyes to prevent dryness and damage to the cornea. After the surface disinfection with iodophor and 70% ethanol, a small incision was made and exposing the skull landmarks lambda and Bregma. Hydrogen peroxide was used to clean the connective tissue. A small hole drilled through the skull with a bone drill. The coordinates of hippocampal were

mediolateral (ML) ± 1.5 mm, anteroposterior (AP) −2.1 mm, dorsoventral 1.8 mm, injected with 1 μL of AAV or/and 3 μL of LV. After injections, the incision was sutured and applied surface disinfection. The mice were monitored 1, 2, 7, and 10 days post-surgery.

Electron microscopy

Mice were perfused with ice-cold 2% glutaraldehyde and 3% paraformaldehyde in PBS. Then hippocampal slices were post-fixed in cold 1% OsO4 for 1 h. Ultrathin sections (90 nm) were stained with uranyl acetate and lead acetate and viewed at 100 kV in a JEOL 200CX electron microscope. Synapses were identified by the presence of synaptic vesicles and postsynaptic densities.

Golgi staining

After perfusion, mice brains were fixed in 10% formalin for 24 h, then put in 3% potassium bichromate for 3 days and change the buffer every day in darkness. After these, the brains were transferred into 2% silver nitrate solution for one week in darkness, change half of the buffer every 3 days. Sections were cut at 50 mm by shock slicer, dehydrated through a discontinuous ethanol gradient: 50%, 70%, 90%, and 100%, then cleared in xylene and coverslipped.

Morris water maze

The water maze is a round, water-filled tank (52 inches diameter), which was surrounded by extra-maze visual cues that kept at the same position during the whole training time. The platform was placed in the NW quadrant of the maze. Water was made with right amount of fat-free milk powder, filled to cover the platform by 1 cm at 22 °C. Each mouse was given 4 trials/day, maximum trial length was 60 s for 5 consecutive days with a 15 min intertrial interval. If mice did not reach the platform in time, they were manually guided to stay on platform for another 10 s. After 5 days of task acquisition, a probe trial was presented. The platform was removed and the percentage of time spent in the quadrant was measured over 60 s. MazeScan (Clever Sys) was used for analyzing all trials latency and swim speed.

Contextual and cued fear conditioning

Mice were placed in a test chamber (7″ W, 7″ D 3 12″ H, Coulbourn) composed of Plexiglass with a metal shock grid floor. After wiped with 70% alcohol, allowed the mice to explore the enclosure for 3 min. Following with 3 conditioned stimulus (CS)-unconditioned stimulus (US) pairings (tone: 2000 Hz, 85-db, 20 s; foot shock: 0.5-mA, 2 s) with a 1 min intertrial interval. One minute following the last CS-US presentation, mice were removed from the chamber. A 24 h later, the mice were presented with a context test, during which subjects were placed in the same chamber used during conditioning on day 1, no shocks were given during the context test. The amount of freezing was recorded. On day 3, a cue test was performed, during which subjects were exposed to the CS in a novel compartment. Animals were allowed to explore the novel context for 2 min, the 85-db tone was presented later. The freezing behavior in the 6 min was recorded via a camera and the software provided by Coulbourn.

Quantification and statistical analysis

In vitro assays, the experiments were conducted by a blind individual, who did not know the sample information. The animal's information for in vivo assays was decoded after all samples were analyzed. Sample size was determined by Power and Precision (Biostat). All data are expressed as mean ± SEM and analyzed by SPSS 12.0 (IBM) and GraphPad Prism statistical software (GraphPad Software). The level of significance between two groups was assessed with unpaired *t* test with Welch's correction. When there are more than two groups, one-way ANOVA and Bonferroni's multiple comparison test was applied. The two-way ANOVA and Bonferroni's post hoc test compared the differences between groups that have been split on two independent factors. A value of $p < 0.05$ was considered to be statistically significant.

Results

TrkB receptors strongly bind to APP

BDNF/TrkB signaling is implicated in AD pathologies, but how the neurotrophic pathway contributes to disease onset remains incompletely clear. To explore whether plasma membrane integral TrkB receptors directly interact with the transmembrane protein APP, we cotransfected GST-APP construct with various HA-tagged tropomyosin receptor kinases plasmids into HEK293 cells, and GST pulldown assay showed that TrkA associated with APP, confirming previous observations [27, 28]. Remarkably, TrkB receptors displayed much stronger effect in binding to APP, whereas TrkC did not interact with APP at all (Fig. 1a). Mapping assay demonstrated that truncating the ICD from either the kinase domain (KD) or SHC-binding motif to the C-terminal on TrkB receptor completely abolished the TrkB/APP complex formation, whereas deletion of the C-terminal PLC binding motif on TrkB tail barely affected the interaction, suggesting that the KD on TrkB ICD is involved in binding APP (Fig. 1b). On the other hand, the reciprocal

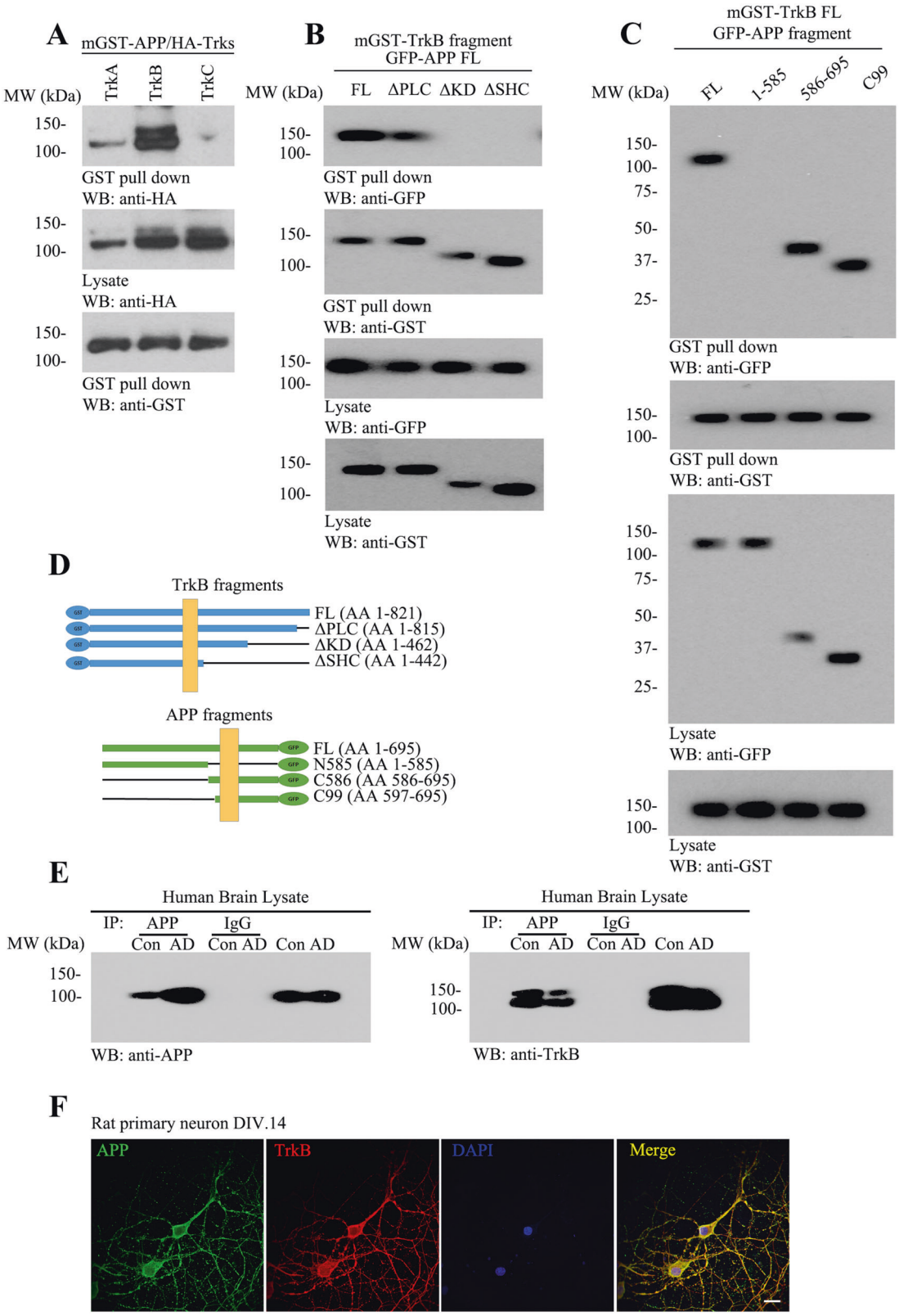

truncation revealed that the intracellular C-terminal domain (ICD) on APP was implicated in association with TrkB (Fig. 1c, d). To investigate whether this interaction also occurs in the brain, we conducted co-immunoprecipitation assay and found that APP and TrkB associated with each other in both control and AD brains; by contrast, control

◀ **Fig. 1 TrkB receptors strongly bind to APP. a** APP specifically interacts with TrkB receptors. GST pull-down assay was conducted from HEK293 cells cotransfected with mammalian GST-APP and HA-Trks constructs. Immunoblotting showed APP interacted with TrkA and TrkB. **b** Tyrosine kinase domain is indispensable for APP to interact with TrkB. GST pull-down assay was conducted from HEK293 cells cotransfected with mammalian GST-TrkB fragments and GFP-APP constructs. Immunoblotting found that TrkB ICD was required for binding to APP. **c** APP C terminus is implicated in binding TrkB. Different mGFP-tagged APP truncates were cotransfected with GST-TrkB into HEK293 cells. GST pull-down assay was performed, and coprecipitated proteins were analyzed by immunoblotting. **d** Schematic diagrams of TrkB domains and APP truncations. **e** APP associates with TrkB less in AD patient brains than healthy control. Brain lysates from AD patient and healthy control were immunoprecipitated with control IgG or anti-APP, and the coprecipitated proteins were analyzed by immunoblotting with anti-TrkB. **f** APP colocalizes with TrkB in the rat primary neurons. Immunofluorescent costaining with anti-APP (Green) and TrkB (Red) were conducted on primary neurons. The nuclei were stained with DAPI. (Scale bar: 20 μm).

IgG failed, indicating that the binding between APP and TrkB was specific. Notably, APP levels were escalated in AD brains, and TrkB receptors were inversely declined in the IP (Fig. 1e). Immunofluorescent (IF) costaining also validated that TrkB and APP colocalized on the cell surface in primary neurons (DIV. 14) (Fig. 1f), supporting that these two transmembrane proteins associate with each other on the plasma membrane of neurons.

BDNF triggers APP Y687 phosphorylation via TrkB receptors

The TrkB receptors are tyrosine kinases and their interaction with APP may phosphorylate the latter. To test this possibility, we conducted cotransfection with GST-APP in the presence of YFP-tagged TrkB wild-type (WT) or kinase-dead mutant (K572R), followed by BDNF treatment. GST pulldown assay showed that APP tyrosine was phosphorylated when cotransfected with TrkB WT, which was elevated upon BDNF treatment. By contrast, no p-Y signals on APP were detected in the presence of TrkB KD regardless of BDNF stimulation. Interestingly, the interaction between TrkB and APP was not influenced by BDNF (Fig. 2a). These observations indicate that TrkB phosphorylates APP on its tyrosine residues, for which its tyrosine kinase activity is indispensable. APP ICD contains 3 Y residues (653, 682, 687) and Y682 is phosphorylated by TrkA [27]. To assess which Y residue is selectively phosphorylated by TrkB, we performed in vitro kinase assay in the presence of [γ-^{32}P]-ATP using synthetic ICD peptide as a substrate. TrkB WT or KD was stimulated with BDNF in the presence or absence of its inhibitor K252a. The active TrkB WT but not KD strongly phosphorylated APP ICD WT, which was completely abrogated with Y687F mutant. Moreover, suppression of TrkB with K252a inhibitor also robustly blunted APP ICD phosphorylation by TrkB WT. TrkB activation was validated by immunoblotting with its autophosphorylation p-Y816 antibody (Fig. 2b). Next, we generated p-APP Y687 rabbit polyclonal antibody, and the specificity of this antibody was confirmed with immunohistochemistry staining (IHC) on mouse forebrain cortex. Prominent p-APP signals were identified by anti-p-Y687 that was selectively blocked by the antigen peptide but not the scrambled peptide (Fig. S1A), suggesting that anti-p-APP Y687 specifically recognizes Y687 phosphorylated APP. The specificity of this antibody was further validated on primary neuronal cultures. As a result, BDNF clearly provoked stronger p-APP Y687 signals than vehicle control, and both APP and p-APP Y687 preferentially distributed in the GGA3 (biomarker for the trans-Golgi network, TGN) versus EEA1 (biomarker for the early endosomes) positive cellular organelles. Anti-p-Y687 and anti-APP spatial distribution tightly coupled with each other (Fig. S1B & C), supporting that p-Y687 antibody selectively recognizes APP in neurons treated with BDNF.

To further assess whether TrkB phosphorylates APP in intact cells, we cotransfected GST-APP WT or Y687F mutant with YFP-tagged TrkB WT or KD plasmid into HEK 293 cells, followed by BDNF stimulation. Immunoblotting revealed that basal p-APP Y687 activities were found in the cells cotransfected with TrkB WT and APP WT. As expected, p-Y687 activities were strongly augmented upon BDNF stimulation, which were mitigated in the presence of either APP Y687F or TrkB KD mutant regardless of BDNF treatment. Again, p-TrkB Y816 autophosphorylation was strongly increased by BDNF, which was totally blunted with TrkB KD (Fig. 2c). Next, we extended our interrogation in vivo and found that deletion of BDNF or TrkB from BDNF f/f mice or TrkB f/f mice completely eradicated p-APP Y687 activities in the mouse brains (Fig. 2d), supporting that BDNF/TrkB signaling is essential for phosphorylation of APP Y687. Since BDNF/TrkB level are reduced in AD patient brains, accordingly, we assessed p-APP Y687 activities on both control and AD patient brain sections. IF costaining showed demonstrable p-Y687 and prominent TrkB signals in control brains, which were evidently attenuated in AD brains (Fig. 2e), indicating that reduced TrkB neurotrophic signaling in AD is unable to trigger APP Y687 phosphorylation.

APP intracellular trafficking and TGN distribution are regulated by TrkB tyrosine kinase

APP trafficking is regulated by its phosphorylation status. To test whether BDNF/TrkB signaling and tyrosine phosphorylation on APP mediates its internalization and subcellular organelle distribution, we conducted p-APP Y687

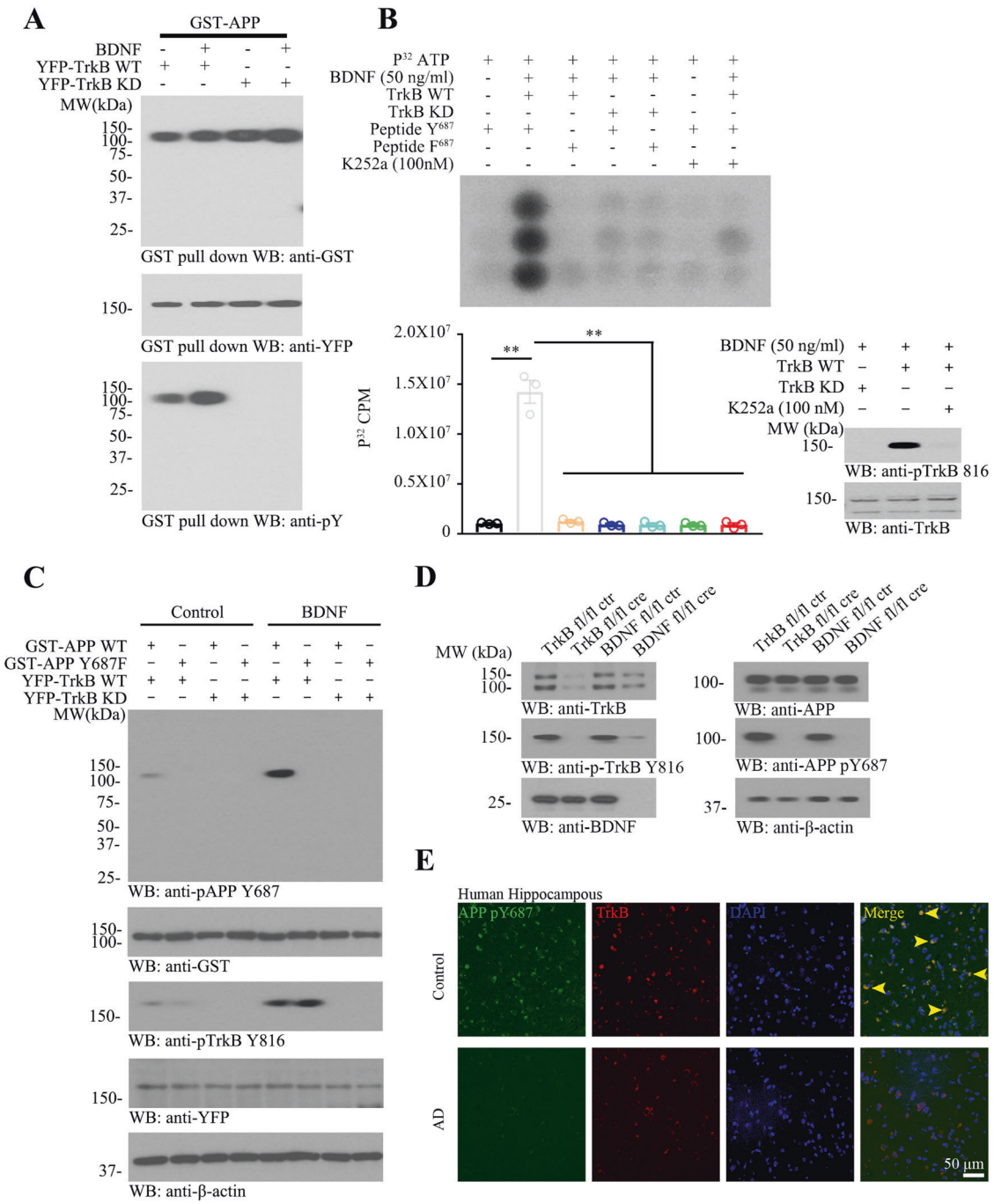

trafficking assay in primary neurons at 4 °C and 37 °C. Anti-APP N-terminal antibody was added into the culture medium to label the extracellular APP on the plasma membrane. If the cultures were kept on ice, internalization did not occur and APP and TrkB costaining was only observed on the cell surface, and APP was barely phosphorylated on Y687. Trivial APP was found in the GGA3 or EEA1 positive organelles (Fig. 3a, upper panels). After BDNF was introduced and the neurons were switched to 37 °C incubator for 1 h, both APP and TrkB surface distribution was conspicuously reduced and p-Y687 signal was elevated. Notably, p-Y687 and APP were both mainly enriched in the TGN, marked with anti-GGA3. They were scarcely resided in the early endosomes (Fig. 3a, lower panels). In contrast, in the presence of PBS control, APP Y687 was barely phosphorylated, though TrkB and APP tightly colocalized in the neurons, and distributed in neither EEA1 or GGA3 positive organelles (Fig. S2A). Thus, TrkB receptor phosphorylates APP on Y687 residue and triggers its internalization induced by BDNF, accumulating in the TGN. To

◀ **Fig. 2 TrkB phosphorylates APP on Y687 residue. a** APP is phosphorylated by TrkB tyrosine kinase. SH-SY5Y cells were cotransfected with YFP-TrkB Wild-type (WT) or Kinase-dead (KD) mutant in the presence of GST-APP, stimulated with or without BDNF (50 ng/ml) for 30 min, GST pulled down complex were monitored by immunoblotting with YFP and p-Tyrosine antibodies. **b** APP Y^{687} is phosphorylated by TrkB receptors. YFP-TrkB WT and KD plasmids were transfected in SH-SY5Y cells and pretreated with/without K252a (TrkB inhibitor, 100 nM) for 15 min, followed by BDNF (TrkB activator, 50 ng/ml) for 30 min. TrkB were pulled down by IP and incubated with Peptide Y^{687} or Peptide F^{687} in a tube with ^{32}P-ATP for 30 min. The 96-well filter plates with negatively charged phosphocellulose were used for the protein kinase assays, the results were shown by autoradiography (upper panel). Quantification of radioactivity on the peptide substrates, data represents mean ± SEM ($n = 3$, $^{**}p < 0.01$, two-way ANOVA and Bonferroni's post hoc test). (Lower left). Effects of BDNF, K252a and purified TrkB were verified by WB (Lower right). **c** APP pY687 is verified by its specific antibody. GST-tagged APP WT or Y687F plasmids were cotransfected with YFP-tagged TrkB WT or KD into SH-SY5Y cells, which were treated with BDNF (50 ng/ml) for 30 min. 48 h later, cells were harvested for WB. **d** APP pY687 is verified by TrkB/BDNF fl/fl cre mice. Age-matched TrkB fl/fl mice and BDNF fl/fl mice were injected with cre virus, the brain lysates were used for verifying the specificity of anti-APP pY687 antibody by WB. **e** APP pY687 is reduced in AD patient hippocampus. Immunofluorescent costaining with anti-APP pY687 (Green) and anti-TrkB (Red) were conducted with human brain sections from healthy controls or AD patients. The nuclei were stained with DAPI (Scale bar: 50 μm).

further examine whether TrkB phosphorylation of APP Y687 mediates its TGN residency, we cotransfected GFP-TrkB WT or KD mutant construct with GST-tagged APP WT or Y687F mutant into neuronal cell line SH-SY5Y, followed by BDNF treatment. As compared with vehicle control, BDNF strongly elicited GST-APP WT but not Y687F mutant to colocalize with GGA3 but not EEA1 in the presence of TrkB WT, and this effect was repressed in the presence of TrkB KD or APP Y687F mutant (Figs. 3b, S2B). Hence, these findings suggest that BDNF activates TrkB receptors that subsequently phosphorylate APP Y687, and p-APP Y687 is preferentially enriched in the GGA3-positive TGN in primary neurons, for which TrkB tyrosine kinase activity is indispensable.

TrkB receptor is cleaved by δ-secretase at N365 and N486/489 sites

We have reported that AEP (asparagine endopeptidase, gene name *LGMN*) acts as δ-secretase, cleaving numerous effectors implicated in AD, including APP, Tau, and SRPK2 etc [24, 25, 29]. Since BDNF/TrkB neurotrophic signaling is involved in AD pathologies, we wondered whether δ-secretase might shred TrkB receptors as well. To figure out this possibility, we conducted an in vitro cleavage assay with GST-TrkB with WT or $LGMN^{-/-}$ brain lysates, prepared under pH 7.4 or 6.0, respectively. Immunoblotting showed that GST-TrkB was potently cleaved by active δ-secretase under pH 6.0 but not 7.4. The proteolytic fragmentation of TrkB was inhibited in LGMN -/- samples regardless of pH 7.4 or 6.0, indicating that TrkB receptors were strongly cleaved by δ-secretase under acidic pH 6.0 (Fig. 4a). To validate that this event was directly executed by δ-secretase, we employed enzymatic-dead C189S mutant or uncleavable mutant N323A (autocleavage of δ-secretase at N323 is required for its activation). As compared with WT δ-secretase, neither C189S nor N323A mutant was able to cut TrkB (Fig. 4b). Moreover, antagonizing δ-secretase with its peptide inhibitor AENK but not the control peptide AEQK strongly blockaded TrkB cleavage (Fig. 4c). Furthermore, δ-secretase antibody but not control IgG dose-dependently blunted TrkB fragmentation, supporting that TrkB proteolytic truncation is specifically conducted by active δ-secretase (Fig. 4d). Endogenous TrkB receptors were also selectively cut in WT but not $LGMN^{-/-}$ mouse brains, lysed in buffer of pH 6.0 but not 7.4 (Fig. 4e), underscoring that δ-secretase is activated under acidic samples and subsequently cleaves TrkB receptors.

To identify the cutting sites on TrkB receptors by δ-secretase, we conducted proteomic analysis to map the potential cutting sites with truncated samples. LC/MS analysis showed that human TrkB N486 and N489 were possible cleavage sites (Fig. 4f). Accordingly, we generated numerous human TrkB point mutants with N into A. As expected, N486A or N489A mutation alone decreased TrkB cleavage but they did not completely block its cleavage at 90 kDa, and N486A/N489A double mutation completely inhibited this fragment production. Surprisingly, N365A mutation strongly inhibited 60 kDa truncate production, though N365 site was not identified in proteomic analysis (Fig. 4g). Presumably, its concentration was not abundant enough to reach the detection threshold by LC/MS/MS. Hence, TrkB receptors can be cleaved in vitro by δ-secretase at N365, N486, and N489 sites. TrkB cleavage assay demonstrated that ~90 kDa band was the most abundant, indicating that N486/N489 location might be the major cutting site on TrkB. Correspondingly, we prepared its rabbit polyclonal antibody. The specificity of this antibody was validated by immunoblotting with samples containing purified GST-TrkB protein cleaved by recombinant δ-secretase. TrkB N486 but not FL TrkB was selectively recognized by this antibody (Fig. S3A). Next, the mouse brains were lysed under pH 7.4 or 6.0, and the endogenous TrkB receptors were selectively cleaved under pH 6.0. The truncated fragments were specifically recognized by rabbit polyclonal anti-N486 and C487 antibodies, respectively, whereas TrkB FL was not recognized by these antibodies, underscoring the specificity of the antibodies (Fig. S3B). We extended our studies into WT and $LGMN^{-/-}$ mice primary neurons, treated with 20 μM Aβ fibrils, and found that Aβ stimulated δ-secretase expression and subsequent

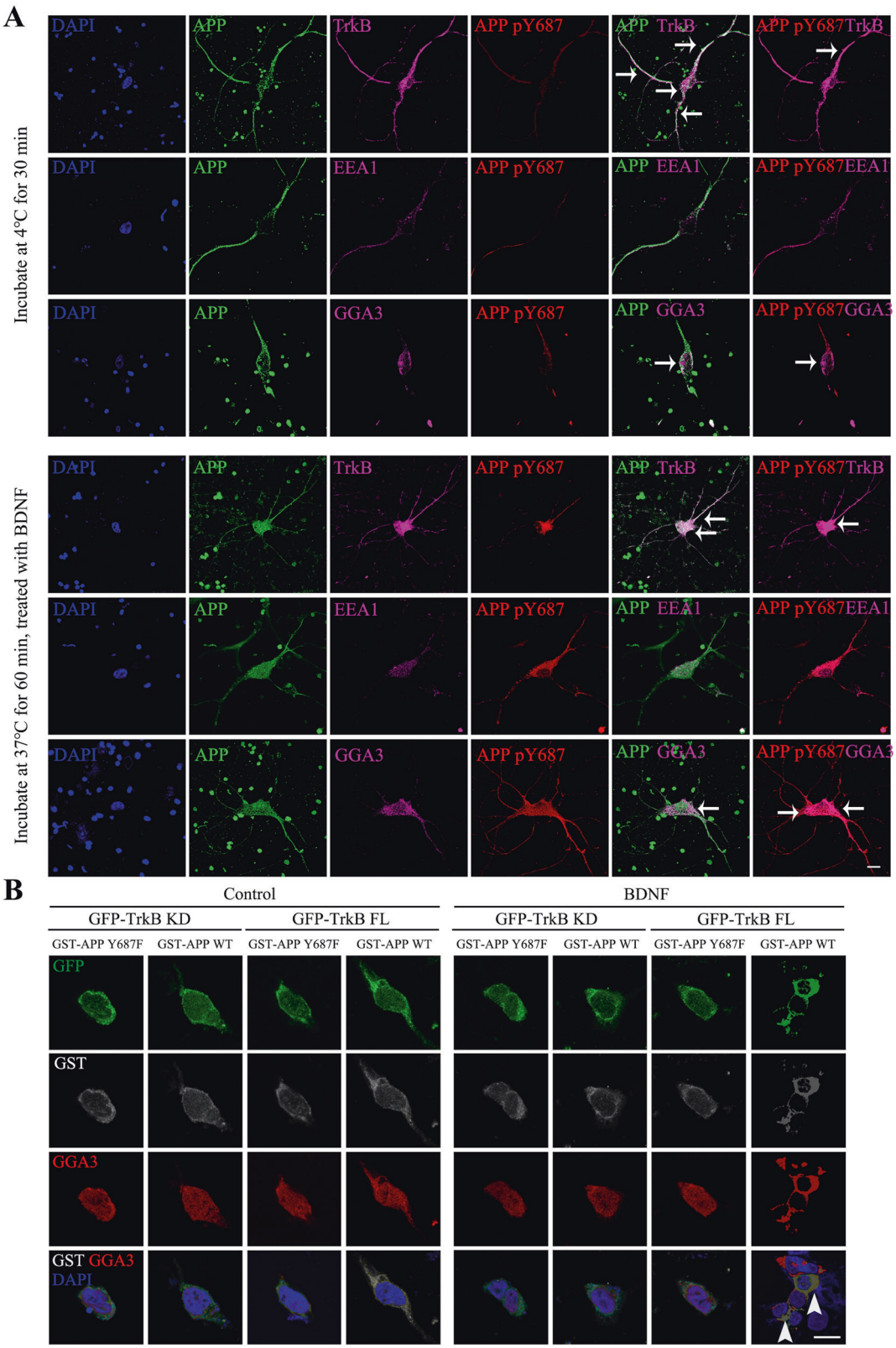

TrkB fragmentation, which was recognized by anti-TrkB N486 antibody in WT but not LGMN-null neurons, supporting that Aβ-activated δ-secretase strongly cuts TrkB at N486 site (Fig. S3C). The antibodies' specificity was further validated by pre-incubation with various peptides. Antigen peptides completely abolished the IHC staining signals of

◀ **Fig. 3 APP Y687 phosphorylation by TrkB receptor regulates APP TGN residency. a** BDNF regulates APP Y687 phosphorylation and intracellular trafficking. Rat primary neurons (DIV. 14) were incubated with APP N terminal antibody (3 μg/ml) at 4 °C for 30 min, and then were treated with BDNF (50 ng/ml) at 37 °C for 1 h. Neurons were fixed and permeabilized, then were incubated with cell organelle markers and APP pY687 antibodies. After incubated with 3 secondary antibodies conjugated with Alexa Fluor™-488, Alexa Fluor™-594, or Cy5 for 1 h respectively, neurons were analyzed under a confocal microscope. EEA1 marked the early endosome, GGA3 marked trans-Golgi network (TGN). The nuclei were stained with DAPI. Arrows indicate the merged part, respectively (Scale bar: 20 μm.). **b** Phosphorylation of APP Y687 mediates its TGN residency. SH-SY5Y cells were cotransfected with TrkB WT or KD construct in the presence of APP WT or Y687F mutant, then treated with or without BDNF (50 ng/ml) at 37 °C for 30 min. Cells were fixed and permeabilized, then incubated with anti-GFP, anti-GST anti-GGA3. After incubated with 3 secondary antibodies conjugated with Alexa Fluor™-488, Alexa Fluor™-594, or Cy5 for 1 h respectively. Cells were analyzed under a confocal microscope. Arrows indicate the merged part (Scale bar: 20 μm).

both anti-N486 and anti-C487, whereas the scramble non-specific peptide failed (Fig. S3D), supporting that both antibodies are specific in recognizing fragmented TrkB receptors cutting at N486 and consequent C487 truncate. Notably, employing the specific antibodies, we found that both TrkB N486 and C487 activities were augmented, albeit TrkB levels were reduced, in AD brains as compared with control brains (Fig. S3E).

To explore whether δ-secretase also cleaves TrkA or TrkC receptors, we performed the similar in vitro cleavage assay. However, only TrkB but not TrkA or TrkC was selectively cut by δ-secretase (Fig. S4A). We also extended our assay into AD mouse model and found that knockout of δ-secretase abolished TrkB fragmentation in 5xFAD mouse brain (Fig. S4B). Our previous study shows that δ-secretase is selectively activated in AD brains but not control brains [25]. As expected, immunoblotting with AD and control brains validated that TrkB receptors were proteolytically cleaved in AD but not control brains (Fig. S4C). IF costaining also supported this observation, as δ-secretase was highly augmented in AD brain, colocalized with TrkB receptors (Fig. S4D).

TrkB receptor is cleaved by active δ-secretase in AD brains

To further explore these biochemical events, we prepared human neurons, induced from healthy control or AD patients' iPSCs. Immunoblotting revealed that TrkB FL was substantially reduced in AD neurons as compared with control neurons, accompanied with escalated 60 kDa TrkB fragment, which was specifically recognized by TrkB N486 antibody. These findings suggest that TrkB receptor was strongly cleaved at N486 site, yielding a 60 kDa band. Interestingly, p-TrkB Y816 signals were evidently decreased in AD neurons versus control neurons. In alignment with these findings, δ-secretase was strongly cleaved in the active form, fitting with its reduced p-T322 activities by Akt. Fitting with TrkB cleavage in AD samples, TrkB receptor lost its tyrosine kinase activity in phosphorylating APP Y687. The unphosphorylated APP was strongly cleaved by active δ-secretase at APP N585 site. In alignment with our previous report, SRPK2 was activated and phosphorylated in AD brains, leading to robust phosphorylation of S226 on δ-secretase (Fig. 5a). To examine the TrkB proteolytic effect in-depth in AD brains, we conducted IF costaining with 3 antibodies. Compared to control brain, δ-secretase was evidently elevated in AD brains and colocalized with APP, which strongly coupled with anti-N486 and anti-C487 signals in AD brain sections that were not detectable in control brains. Moreover, δ-secretase also colocalized with truncated TrkB N486 or C487 fragments but not TrkB FL in AD brains (Fig. 5b). Since BDNF is reduced in AD brains, we assessed whether BDNF deprivation could recapitulate these biochemical effects in primary neuronal cultures. Immunoblotting revealed that anti-BDNF completely antagonized p-TrkB Y816 signals, associated with prominent δ-secretase activation. Consequently, TrkB N486 was intensely cleaved, so were other well-characterized δ-secretase substrates including APP N585, Tau N368. It was worth noting that sAPPβ from BACE1 was also robustly elevated, when BDNF was neutralized by its specific antibody (Fig. 5c). In alignment with these findings, δ-secretase was significantly activated upon BDNF deprivation (Fig. 5d). Quantitative analysis showed that both Aβ40 and 42 levels were augmented when BDNF was antagonized (Fig. 5e). Hence, TrkB receptors are predominantly cleaved at N486 site by δ-secretase in AD.

Delta-secretase is physiologically sequestered in the endo-lysosomes, and it is activated only under acidosis. We have reported that SRPK2 phosphorylates δ-secretase S226 and elicits its cytoplasmic translocation and activation [30]. To explore whether this post-translational modification alters δ-secretase enzymatic activation profile under different pH values, we transfected GST-δ-secretase WT or S226D mutant (phosphorylation mimetic) or cotransfected δ-secretase WT or unphosphorylate S226A mutant with SRPK2. Immunoblotting revealed that GST-δ-secretase was phosphorylated on S226 by SRPK2 (Fig. S5A). The cotransfected cells were lysed under different pH buffers, and δ-secretase enzymatic assay showed that its activities gradually declined as the pH values progressively escalated, and minimalized at pH 7.0. Strikingly, phosphorylation mimetic S226D mutant or δ-secretase WT cotransfected with SRPK2 exhibited significantly higher enzymatic activity at pH 7.5 than other conditions (Fig. S5B & C),

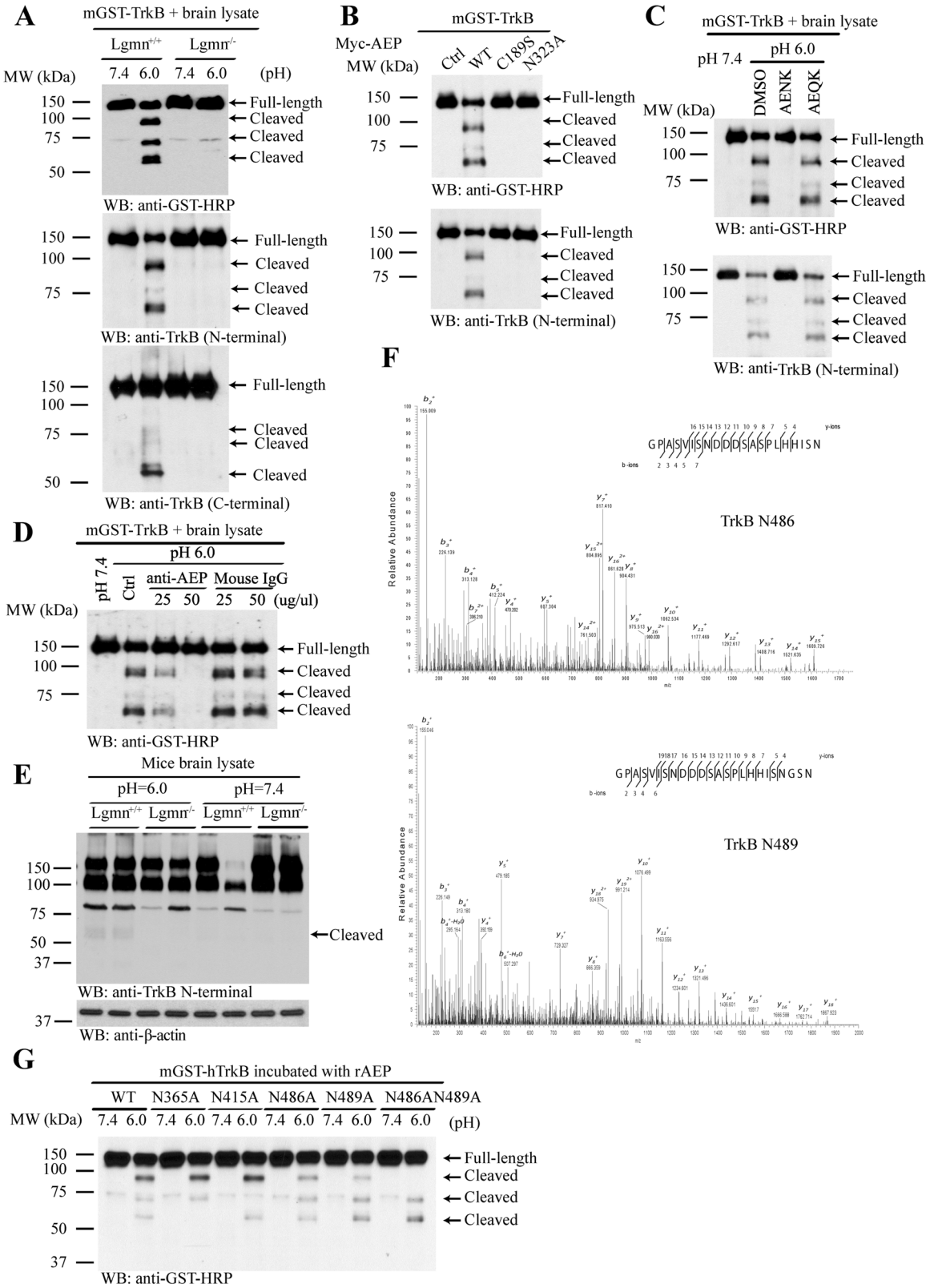

suggesting that p-S226 modification maintains δ-secretase activity even at pH 7.5. Quantitative analysis demonstrated that δ-secretase S226D revealed higher enzymatic activity than WT counterpart, and WT displayed higher activities than S226A in the presence of SRPK2 under both pH 7.4 and 6.0, though the former were weaker than the latter

◀ **Fig. 4 TrkB is truncated by δ-secretase at N365 and N486/489 sites. a** TrkB cleaved by δ-secretase. Western blot showed the cleavage of GST-TrkB, GST-TrkB were purified by GST pulldown from transfected HEK293 cell lysates, then TrkB were incubated with brain lysates from $Lgmn^{+/+}$ or $Lgmn^{-/-}$ mice at pH 7.4 or pH 6.0, respectively. **b** Western blot showed TrkB was cleaved by WT but not enzymatic-dead or N323A mutated AEP constructs. **c** AEP peptide inhibitor blocks TrkB cleavage by δ-secretase. Western blot showed the competition effect of AENK and AEQK on TrkB cleavage. **d** Antibody titration assay showed TrkB cleaved by δ-secretase. Mouse IgG was used as negative control. AEP antibody dose-dependently neutralized TrkB cleavage in the lysates. **e** Western blot showed the cleavage of endogenous TrkB by δ-secretase in mouse brains. **f** Mass spectrometry analysis of recombinant TrkB fragmented by δ-secretase. The detected tandem mass spectrometry peptide spectra were listed. **g** Cleavage of purified human TrkB by recombinant δ-secretase (rAEP). TrkB cleavage was analyzed by Western blot after purified TrkB WT or mutants were incubated with rAEP. Western blot data are representative of three independent experiments.

(Fig. S5D & E). To assess the potential subcellular locations where active δ-secretase cleaves TrkB receptor in primary neurons, we conducted IF costaining with TrkB and δ-secretase in the presence of LE-28, a fluorescent dye that lights up upon active δ-secretase cleavage of the conjugated peptide [31]. Consequently, primary neurons were treated with Aβ to trigger δ-secretase activation, followed by IF costaining analysis. Active δ-secretase, as validated by fluorescent LE-28, colocalized with TrkB receptor in primary neurons, and cleaved TrkB N486 fragment was confirmed by the costaining with the cleavage specific antibody (Fig. S5F–I). Hence, these data support that δ-secretase predominantly cleaves TrkB receptors at N486 site.

To further assess the role of BDNF/TrkB signaling in APP and δ-secretase crosstalk, we conducted IF costaining assay. Under basal control in primary neurons, endogenous δ-secretase was colocalized with APP, justifying that their enzyme/substrate relationship. Nevertheless, endogenous δ-secretase was clearly reduced and p-APP Y687 robustly elevated upon BDNF treatment. Markedly, δ-secretase was segregated from APP and p-APP (Fig. S6A). To explore the subcellular location where TrkB and APP were proteolytically cleaved by active δ-secretase, we conducted subcellular fractionation with 9-month old WT mouse brains or 5xFAD brains. Immunoblotting showed that δ-secretase mainly distributed in WT brain from fraction #6-11, cofractionated with LAMP1 positive lysosomes, and the majority of active δ-secretase localized in fraction #9 and #11. Interestingly, TrkB FL was allocated in two parts from fraction #5-7 and #10-13; and truncated TrkB N486 was allotted from fraction #9-11, cofractionated with active δ-secretase. Notably, p-APP Y687 and APP principally resided in fraction #4-6, cofractionated with GGA3 and EEA1and LAMP1 positive organelles. By contrast, δ-secretase expression levels were highly escalated and distinctly activated in 5xFAD brains. They were allocated from fraction #3-13 with the active fragments enriched from fraction #3-5 and #9-13. Strikingly, TrkB FL were palpably decreased and condensed in fraction from #6-10, whereas TrkB N486 fragments were dispersed in fraction #5 and fraction #9-12. Strikingly, p-APP Y687 was barely detectable, though APP levels were increased in 5xFAD mouse brains (Fig. S6B). To investigate the biological functions of TrkB fragments, we infected AAV virus expressing GFP-tagged TrkB truncates into primary neurons and treated the cells with PBS or BDNF. Immunoblotting showed that p-Y816 signal on endogenous TrkB receptor was totally inhibited by GFP-TrkB N486 regardless of BDNF or PBS treatment, whereas p-TrkB Y816 activities remained comparable in other groups. The downstream p-Akt S473 oscillated with the upstream p-TrkB activities (Fig. S6C). To further explore the fragments' biochemical effects, we purified GST-tagged recombinant proteins and introduced them into primary neuronal cultures. IF costaining showed that GST-TrkB N486 truncate but not other fragments strongly induced TUNEL-positive neuronal apoptosis (Fig. S6D & E). Quantification assays of abnormal neuronal morphology and apoptosis demonstrated that inhibition of BDNF signaling by TrkB N486 truncate potently elicited neurotoxicity and neuronal cell death (Fig. S6F).

Delta-secretase-uncleavable TrkB N486/489 A attenuates AD pathologies in 5xFAD mice

TrkB receptors are potently cleaved in both 5xFAD and human AD patient brains, attenuating neurotrophic activities. To investigate the in vivo effects of blocking TrkB fragmentation by δ-secretase, we injected AAV virus expressing GFP-tagged TrkB WT or δ-secretase-uncleavable TrkB N486/489 A mutant into the hippocampus of 2 months old 5xFAD mice. In 4 months, we analyzed the expression of infected constructs and found that exogenously administrated TrkB was potently expressed and TrkB N486 was robustly cleaved in control virus injected brains, whereas this fragment was barely detectable in TrkB WT or N486/489 A mutant overexpressed brains. TrkB N486 fragmentation pattern correlated with δ-secretase activation. In alignment with the upstream robust p-TrkB Y816 activities, p-APP Y687 was the strongest in TrkB N486/489 A samples, followed by TrkB WT brains, but it was not demonstrable in control brains. Consequently, δ-secretase-cleaved APP N585 levels and β-secretase-cleaved sAPPβ levels were inversely coupled with p-APP Y687 signals (Fig. 6a). Thus, protection of TrkB from δ-secretase cleavage elevates TrkB activation, resulting in potent p-APP Y687 activities and prevention of APP N585 and sAPPβ proteolytic truncation. Quantitative analysis showed that δ-secretase enzymatic activities were decreased in TrkB WT and N486/489 A mutant samples as

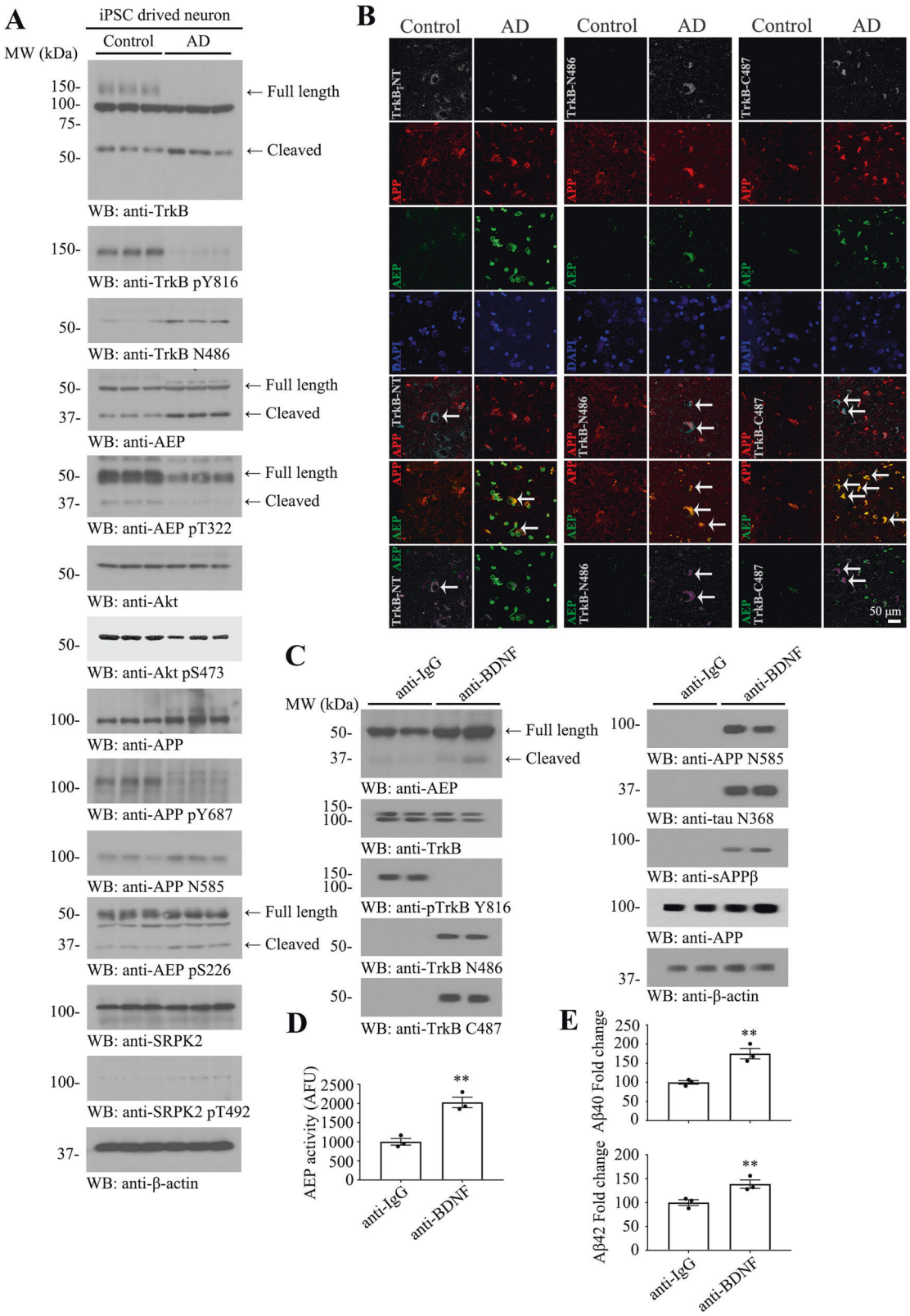

compared with control with the latter significantly lower than the former. In accord with APP N585 fragmentation activities, both Aβ40 and 42 concentrations were substantially reduced in the brains expressing TrkB WT and N486/489 A mutant (Fig. 6b). IHC and Thioflavin S (ThS) costaining revealed a large number of aggregated Aβ

◀ **Fig. 5 TrkB receptors are cleaved by δ-secretase in AD brains, abolishing APP Y687 phosphorylation. a** TrkB and APP are cleaved by active δ-secretase in AD human neurons. The human iPSC-derived neurons from healthy control and AD patients were harvested for the WB and detected with various indicated antibodies. **b** Truncated TrkB 1-486 and 487-822 fragments are increased in AD patient hippocampus. Immunofluorescent costaining with anti-TrkB (Gray), APP (Red), and AEP (Green) were conducted with human brain sections from healthy control or AD patient. The nuclei were stained with DAPI. Arrows indicate the merged part (Scale bar: 50 μm.). **c** Deprivation of BDNF increases cleavage of TrkB by δ-secretase. Immunoblotting were conducted from rat primary neurons after incubation with anti-BDNF or anti-IgG antibodies. Data are representative of three independent experiments. **d** BDNF deprivation increases AEP enzymatic activity. The same samples come from C were used to perform the AEP activity assay. Data represent mean ± SEM ($n = 3$, $^{**}p < 0.01$, unpaired t test with Welch's correction). **e** BDNF deprivation stimulates Aβ production. Quantification of Aβ40 and Aβ42 levels by ELISA represents mean ± SEM ($n = 3$, $^{**}p < 0.01$, unpaired t test with Welch's correction).

plaques that were greatly diminished in TrkB WT and N486/489 A mutant brain sections (Fig. 6c). The dendritic spines showed in Golgi staining were increased most in N486/489 A mutant expressing brains, followed by TrkB WT, as compared with control (Fig. 6d). Electron microscopy (EM) analysis demonstrated that the synapses were enhanced in the similar pattern to that of dendritic spines (Fig. S7A & B). These findings support that overexpression of δ-secretase-uncleavable TrkB N486/489 A considerably escalates the synaptic plasticity. Morris Water Maze (MWM) cognitive behavioral assays supported the latency was significantly reduced in TrkB WT and N486/489 A mutant expressed mice as compared with control 5xFAD mice in the learning trials. After the submerged platform was removed, TrkB N486/489 A mice spent most of time in the target quadrant, followed by TrkB WT mice, compared with control mice in the memory test (Fig. 6e). The swim speed and AUC latency remained comparable among the groups, indicating that the motor functions for these mice were similar (Fig. S7C). Fear conditioning test revealed that TrkB N486/489 A mice displayed the best memory, followed by TrkB WT, as compared with control mice in both Contexual fear freezing and cued fear freezing assays (Fig. 6f). Hence, these findings support that blockade of TrkB from δ-secretase cleavage strongly mitigates APP cleavage and reduces Aβ production and aggregation, leading to restoration of cognitive functions.

Delta-secretase-truncated TrkB fragment facilitates AD pathologies in APP/PS1 mice

The above biochemical studies demonstrate that TrkB N-terminal 1-486 fragment from δ-secretase cleavage blocks BDNF signaling and induces neuronal cell death. To dig out the pathological role of this event in vivo, we employed APP/PS1 mice that display AD pathologies and cognitive dysfunction at age of 12 months or older. We injected AAV virus expressing GFP-tagged TrkB 1-486 or FL into the hippocampus of 2 months old APP/PS1 mice, and conducted immunoblotting assay 4 months later. TrkB WT and 1-486 fragment were highly expressed in the brains. Interestingly, TrkB WT mice exhibited higher p-TrkB 816 signals than control mice, which were completely blunted by 1-486 truncate. Fitting with these findings, p-APP Y687 was greatly elevated in TrkB WT brains. Noticeably, δ-secretase cleavage and activation were stronger in 1-486 brains than control; in contrast, δ-secretase cleavage/activation was evidently suppressed in TrkB WT brains. In consequence, APP N585 fragmentation and β-secretase-cleaved sAPPβ levels correlated with δ-secretase activation status, which were inversely coupled with p-APP Y687 signals (Fig. 7a). Quantitative assays showed that δ-secretase enzymatic activities were highly augmented in 1-486 brains and significantly repressed in TrkB WT brain as compared with the control. Aβ40 and 42 concentrations exhibited the similar pattern (Fig. 7b). IHC and ThS costaining showed that Aβ signals and ThS positive plaques were abundantly increased in TrkB 1-486 expressed APP/PS1 brains, which were attenuated in TrkB WT brains as compared with control (Fig. 7c). In alignment with these amyloid pathologies, Golgi staining and EM analysis demonstrated that the dendritic spines and synapses were more copious in TrkB WT brains than controls, whereas the 1-486 brains exhibited the fewest (Figs. 7d; S8A & B). MWM cognitive tests revealed that TrkB WT mice revealed significantly better learning and memory capabilities than control mice, while 1-486 mice displayed the poorest performance (Fig. 7e), though these rodents exhibited comparable swim speeds and escape latency, indicating their locomotive functions remain intact (Fig. S8C). Fear conditioning tests demonstrated the same learning and memory manner as MWM cognitive behaviors (Fig. 7f). Therefore, TrkB 1-486 overexpression antagonizes BDNF/TrkB neurotrophic signaling and activates δ-secretase, resulting in p-APP Y687 attenuation and APP N585 fragmentation augmentation, which in turn accelerate amyloid pathologies and cognitive disorders in APP/PS1 mice.

Discussion

In this study, we show that TrkB robustly binds to APP and subsequently phosphorylates Y687 residue, which regulates its TGN residency and diminishes the proteolytic cleavage, leading to attenuation of Aβ production. Currently, it remains unclear whether other kinases besides TrkB could also phosphorylate APP Y687. Remarkably, δ-secretase cleaves TrkB receptor on both extracellular domain and

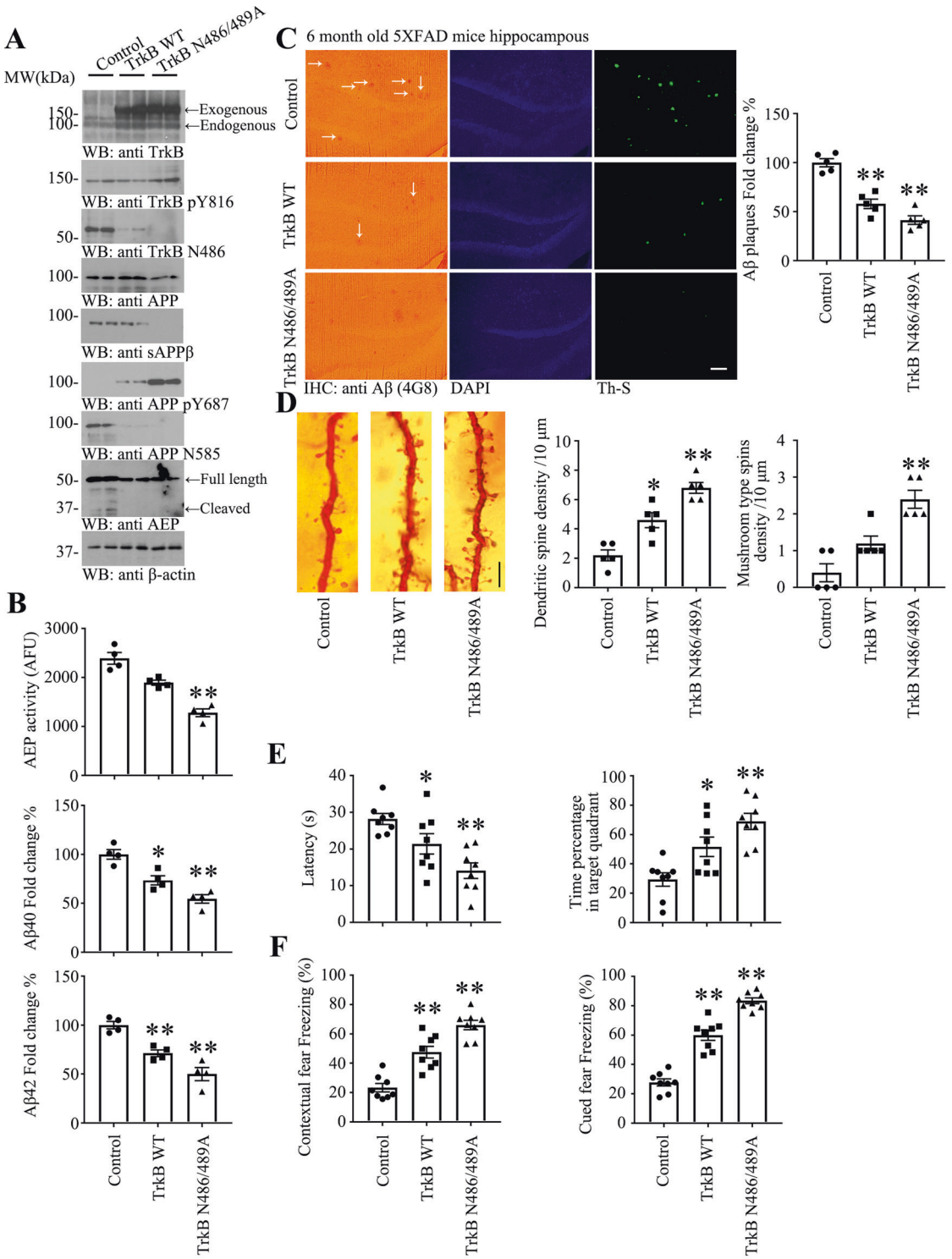

ICD at N365 and N486/489 sites, respectively, abolishing BDNF/TrkB neurotrophic signaling. Recently, we have reported that δ-secretase cuts APP on the extracellular domain at N373 and N585 residues, yielding a better substrate (APP 586-695, C110 fragment) to allow BACE1 to produce Aβ more efficiently. We show that δ-secretase distributes in the endo-lysosomes, cofractionated with APP in AD brains, truncating the endocytosed APP in the acidic endo-lysosomal organelles [24]. Here we show that TrkB receptors are evidently reduced in 5xFAD mouse brains as compared with WT mice, and active δ-secretase cofractionated with truncated TrkB N486. Noticeably, p-APP Y687

◀ **Fig. 6 δ-secretase-resistant TrkB N486/489 A mutant attenuates AD pathologies in 5xFAD mice. a** Uncleavable TrkB N486/489 A inhibits δ-secretase activation. Western blot analysis of TrkB, APP, δ-secretase cleavage in 6-month old 5xFAD mice CA1 infected with lentivirus expressing TrkB FL or δ-secretase-uncleavable TrkB mutant (N486/489 A) for 3 months. Blocking of TrkB cleavage by δ-secretase reduced δ-secretase itself cleavage. **b** Uncleavable TrkB N486/489 A decrease AEP activity and Aβ production. δ-secretase activity was decreased in uncleavable TrkB-expressed 5XFAD mice. Data represent mean ± SEM. ($n = 4$, $^{**}p < 0.01$, compared with control, one-way ANOVA and Bonferroni's multiple comparison test). Aβ level was decreased in TrkB N486/489A-expressed 5XFAD mice. Quantification of Aβ40 and Aβ42 levels by ELISA represents mean ± SEM ($n = 4$, $^{*}p < 0.05$, $^{**}p < 0.01$, compared with control, one-way ANOVA and Bonferroni's multiple comparison test). **c** Aβ plaques in the hippocampus were decreased with overexpression of TrkB N486/489 A. Immunohistochemistry (IHC) staining of Aβ (left) and Thioflavin S staining (right) showed the Aβ plaques in the hippocampus (Scale bar: 100 μm), arrows showed the Aβ plaques. Quantification of Aβ plaques showed amyloid plaques were decreased in TrkB N486/489A-expressed 5XFAD mice. (mean ± SEM; $n = 5$, $^{**}p < 0.01$, compared with control, one-way ANOVA and Bonferroni's multiple comparison test). **d** Blocking TrkB cleavage by δ-secretase rescues the loss of dendritic spine density. Left, Golgi staining was conducted on brain sections from TrkB WT or N486/489 A expressed apical dendritic layer of the CA1 region (Scale bar: 10 μm). Right, quantification of spine density and mushroom type spins density, represents mean ± SEM of 9–12 sections from 5 mice in each group. ($^{*}p < 0.05$, $^{**}p < 0.01$, compared with control, one-way ANOVA and Bonferroni's multiple comparison test). **e** Morris Water Maze analysis of cognitive functions. Uncleavable TrkB expression in the CA1 reversed the learning and memory dysfunctions in 5XFAD mice (mean ± SEM.; $n = 8$ mice per group; $^{*}p < 0.05$, $^{**}p < 0.01$, compared with control, one-way ANOVA and Bonferroni's multiple comparison test). **f** Fear condition tests. Contextual and cued fear memory was rescued in uncleavable TrkB expressed mice (mean ± SEM; $n = 8$ mice per group; $^{**}p < 0.01$, compared with control, one-way ANOVA and Bonferroni's multiple comparison test).

activities were prominent in WT mouse brains, but they were barely detectable in age-matched 5xFAD mice (Fig. S6B), fitting with impaired BDNF/TrkB signaling in AD brain.

The δ-secretase enzymatic activity is pH-dependent and mediated by acidosis [32]. To explore whether cytosolic leaked δ-secretase is still active and cutting its substrates, we have examined its enzymatic activity in primary neurons treated with Aβ, with a specific fluorescent dye LE-28 that lights up upon cleavage by active δ-secretase [31] (Fig. S5F-I). This finding suggests that δ-secretase is still enzymatically active even outside of the acidic endo-lysosome organelles. We validated that δ-secretase actively cleaved TrkB receptors in primary neurons, colocalizing with truncated TrkB N486 (Fig. S5H). On the other hand, it could also shred TrkB receptors at N365, after they are endocytosed in the endo-lysosomes, as revealed in the cofractionation from the AD brains (Fig. S6B). We have previously reported that SRPK2 and Akt phosphorylate δ-secretase on S226 and T322 residues, respectively, and regulate its subcellular residency and enzymatic activities [26, 30]. SRPK2 phosphorylation of S226 on δ-secretase elicits its cytoplasmic translocation from the lysosomes, and active δ-secretase may cleave TrkB N486/489 residues on the intracellular domain, abrogating BDNF neurotrophic signaling. Surprisingly, SRPK2-phosphorylated δ-secretase is active even under neutral pH 7.5 (Fig. S5). This observation is in alignment with our previous findings. For instance, we have previously reported δ-secretase's numerous cytoplasmic substrates including Tau, α-Syn and SRPK2 [24, 25, 33]. Furthermore, δ-secretase is a secreted protease [34] and it also colocalizes with TrkB receptors in primary neurons and AD brains (Figs. S5 & S6). Conceivably, δ-secretase might cut both N365 site on TrkB receptor and N373 and N585 sites on APP extracellularly after secretion. Our previous studies with δ-secretase inhibitor show that compound 11 is orally bioactive and exhibits negligible toxicities after chronic oral administration [33]. Imaginably, δ-secretase inhibitors may possess tremendous therapeutic potential for treating AD. They not only directly block APP and Tau fragmentation and display the disease-modifying effects but also protect BDNF/TrkB neurotrophic activities via inhibiting TrkB truncation from active δ-secretase. The latter will subsequently result in promoting neuronal survival and augmentation of synaptic plasticity.

The intracellular region of APP harbors eight putative phosphorylation sites and is functionally important. Of these, seven (Y653, S655, T668, S675, Y682, T686, and Y687) are phosphorylated in the brains of AD patients [35]. Numerous proteins bind this region of APP and regulate its proteolytic processing and functions [36]. Most interactions involve the YENPTY sequence (amino acids 682–687) on APP. For example, APP Y682 phosphorylation mediates development [37] and APP processing [38]. Furthermore, some proteins interact with APP is dependent on p-Y682 status [39, 40]. However, we found that the interaction between TrkB and APP is independent of APP tyrosine phosphorylation, as both WT or kinase-dead TrkB display comparable binding activities toward APP regardless of BDNF treatment, though the APP p-Y signals are strongly escalated upon BDNF treatment (Fig. 2a). These observations suggest that BDNF strongly stimulates TrkB to phosphorylate APP Y687. It remains elusive whether the association of TrkB with APP detected by co-IP is indirect or direct. However, the finding that TrkB can directly phosphorylate APP in vitro and in vivo (Fig. 2), supporting that their association might be direct.

Previous reports show that overexpression of the TrkA triggers phosphorylation of APP on Y682 and alters its processing, suggesting that tyrosine phosphorylation of APP may functionally link APP processing and neurotrophic signaling to intracellular pathways associated with cellular differentiation and survival [41]. In alignment with these results, we find that p-APP Y687 by TrkB tyrosine

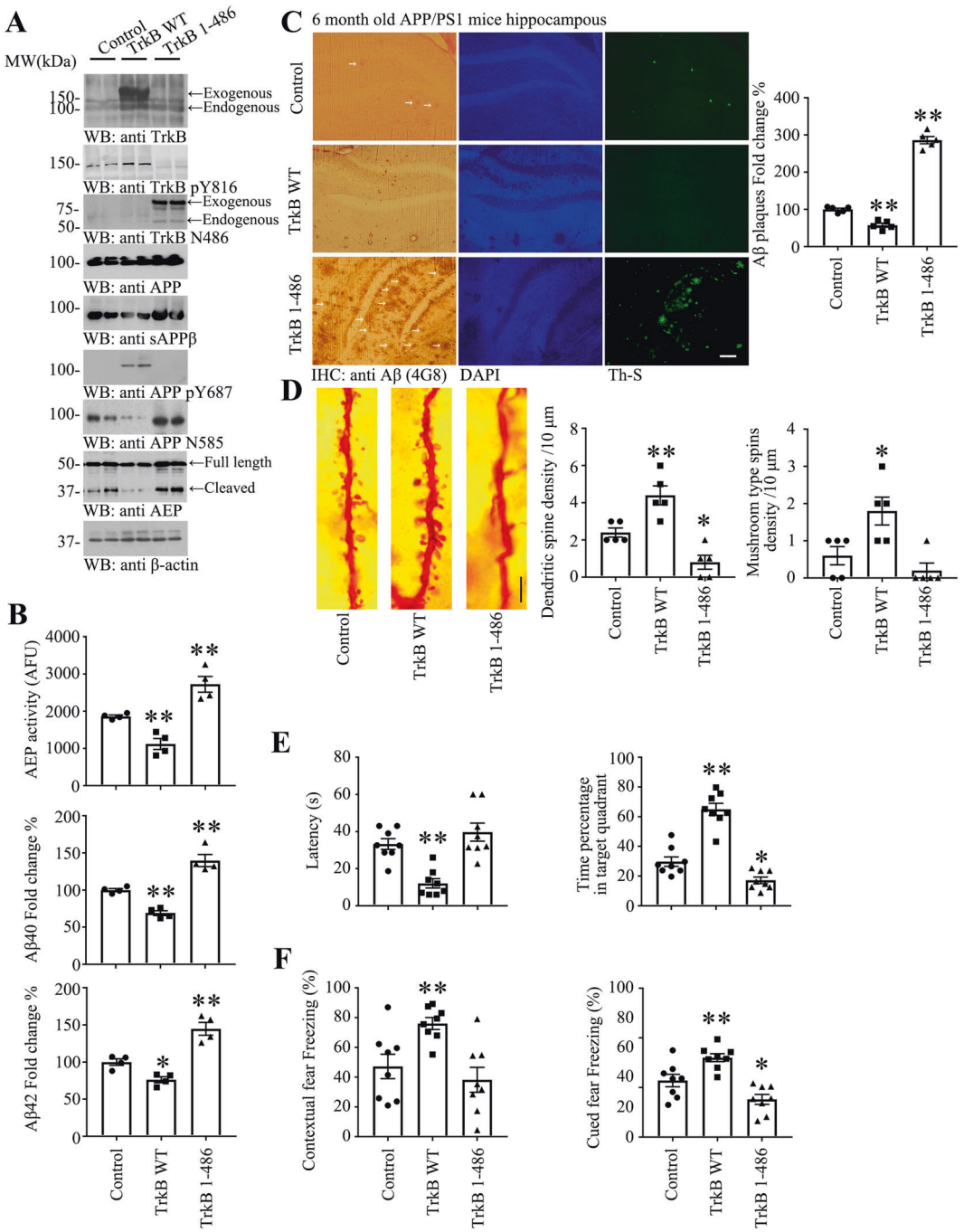

kinase strongly represses APP proteolytic processing, resulting in Aβ production reduction. Accordingly, when TrkB receptors are shredded in AD brains by active δ-secretase, p-APP Y687 signals are evidently mitigated (Fig. 5), which is tightly correlated with escalated APP N585 cleavage by δ-secretase and augmented Aβ production in AD brains (Figs. 6 & 7). Employing viral administration to express δ-secretase-uncleavable TrkB N486/489 A in acute 5xFAD model, we provide the loss-of-function evidence that blockade of TrkB proteolytic cleavage by δ-secretase elevates p-APP Y687 and p-TrkB Y816 and represses δ-secretase activation, leading to inhibition of APP cleavage and Aβ production. Compared with control or TrkB WT overexpressed 5xFAD mice, TrkB N486/489 A significantly alleviates AD pathologies and restores cognitive functions (Figs. 6 & S7). While reduction of Aβ is one potential contributor to these effects, increased TrkB activity could also be contributing to these effects through non-Aβ mechanisms. For example, BDNF stimulation increases synaptic spine density by the mechanisms

◀ **Fig. 7 TrkB 1-486 fragment from δ-secretase cleavage accelerates AD pathologies in APP/PS1 mice. a** TrkB 1-486 expression induces δ-secretase activation and APP cleavage. Western blot analysis of TrkB, APP and AEP cleavage by δ-secretase in 6-month old APP/PS1 mice CA1 infected with lentivirus expressing TrkB WT or fragment for 3 months. δ-secretase-cleaved TrkB fragment stimulated δ-secretase cleavage in the brains. **b** AEP enzymatic and Aβ ELISA assays. δ-secretase activity was increased in TrkB 1-486-expressed APP/PS1 mice CA1. Truncated TrkB escalated δ-secretase activities. Data represent mean ± SEM of 4 mice in each group (**$p < 0.01$, compared with control, one-way ANOVA and Bonferroni's multiple comparison test). Truncated TrkB escalated Aβ level. Quantification of Aβ40 and Aβ42 levels by ELISA represents mean ± SEM ($n = 4$, *$p <$ 0.05, **$p < 0.01$, compared with control, one-way ANOVA and Bonferroni's multiple comparison test). **c** Immunohistochemistry (IHC) staining of Aβ (left) and Thioflavin S staining (right) showed the Aβ plaques in the hippocampus (Scale bar: 100 μm.), arrows showed the Aβ plaques. Quantification of Aβ plaques showed amyloid plaques were increased in TrkB 1-486-expressed APP/PS1 mice. (mean ± SEM; $n = 5$, **$p < 0.01$, compared with control, one-way ANOVA and Bonferroni's multiple comparison test). **d** TrkB cleavage by δ-secretase decreases the dendritic spine density. Left, Golgi staining was conducted on brain sections from TrkB WT or 1-486 expressed apical dendritic layer of the CA1 region (Scale bar: 10 μm). Right, quantification of spine density and mushroom type spins density, represents mean ± SEM of 9–12 sections from 5 mice in each group. (*$p < 0.05$, **$p < 0.01$, compared with control, one-way ANOVA and Bonferroni's multiple comparison test). **e** Morris Water Maze analysis of cognitive functions. TrkB 1-486 overexpression in the CA1 exacerbated the learning and memory dysfunctions in APP/PS1 mice (mean ± SEM; $n = 8$ mice per group; *$p < 0.05$, **$p < 0.01$, compared with control, one-way ANOVA and Bonferroni's multiple comparison test). **f** Fear condition tests. Contextual and cued fear memory was reduced in AEP-truncated TrkB expressed mice (mean ± SEM; $n = 8$ mice per group; **$p < 0.01$, compared with control, one-way ANOVA and Bonferroni's multiple comparison test).

dependent on the Ras/ERK pathway [42] and TRPC3 [43]. Moreover, BDNF regulates p21-activated kinase and ADF (actin-depolymerizing factor)/cofilin, mediates the theta burst stimulation-induced increase in actin polymerization in dendritic spines [44]. On the other hand, we also provide the gain-of-function by viral expression of TrkB 1-486 fragment in the relatively slow APP/PS1 mouse model. In alignment with TrkB 1-486's neurotoxicity by neutralizing BDNF (Fig. S6), we show that TrkB 1-486 overexpression completely abolishes p-APP Y687 and strongly activates δ-secretase, which stimulates robust APP cleavage and Aβ production escalation, resulting in acceleration of AD pathologies and exacerbation of cognitive dysfunction (Fig. 7). Moreover, increased Aβ activates δ-secretase [24] and subsequently triggers the δ-secretase-TrkB-APP-Aβ-δ secretase loop, which further increases the risk of AD.

In addition to Y682, previous studies show that NGF also regulates APP phosphorylation at T668, a key modification that control APP trafficking. NGF withdrawal results in the increase of p-T668 levels in PC12-derived neurons while exposure to NGF reduces p-T668 levels in primary neurons [45]. NGF promotes TrkA binding to APP and APP trafficking to the Golgi, where APP-BACE interaction is hindered, resulting in reduced generation of sAPPβ, CTFβ, and Aβ42. These results demonstrate that NGF signaling directly controls basal APP phosphorylation, subcellular localization and BACE cleavage in AD therapy [45]. In alignment with these results, we demonstrate that BDNF-triggered p-APP Y687 is principally resided in the TGN (Fig. 3). These findings are consistent with previous report. For instance, phosphorylation mimetic APP Y687E-GFP is targeted to the membrane but cannot be detected in transferrin containing vesicular structures, and exhibits a concomitant and dramatic decrease in Aβ production. In contrast, unphosphorylated APP Y687F-GFP is endocytosed similarly to WT APP, but is relatively favored for BACE cleavage. Therefore, Y687 is a critical residue determining APP targeting and processing via different pathways, including endocytosis and retrograde transport [46]. Interestingly, APP Y687F mutant possesses shorter half-life and exits from the TGN, when compared with APP WT or Y687E mutant, which is significantly retained both in the ER and TGN. In addition, this mutant is not incorporated into visible vesicular structures, with a concomitant dramatic decrease in Aβ production [47]. Hence, phosphorylation of APP on Y687 by TrkB is an important regulatory mechanism in terms of determining the subcellular localization of APP and modulating its processing via different proteolytic pathways. This observation fits with previous notion that the endocytic trafficking of APP facilitates amyloidogenesis, while at the cell surface, APP is predominantly processed in a non-amyloidogenic manner [48]. Though both NGF/TrkA and BDNF/TrkB pathways mediate Aβ production via phosphorylating APP and dictating its subcellular trafficking, it remains obscure where in the brain and at what stage do neurotrophine deficiency contributes to AD pathology onset. The crosstalk between TrkA and TrkB receptors with APP and their intracellular trafficking and proteolytic cleavage by δ-secretase are depicted in the schematic model of Fig. S9. Nonetheless, BDNF/TrkB distribution is much broader than NGF/TrkA in the CNS and the former pathway tightly regulates δ-secretase via direct phosphorylation by its downstream signaling. Moreover, δ-secretase selectively cleaves TrkB but not TrkA, in addition to truncation of both and APP and Tau. Conceivably, BDNF/TrkB signaling plays a more important role in AD pathogenesis.

In the current research, we provide compelling evidence showing that TrkB robustly binds APP and phosphorylates its Y687 residue, triggering its TGN accumulation and reduction of amyloidogenic cleavage. Noticeably, p-Y687 is strongly reduced in human AD brains and 5xFAD mice (Figs. 2e, S6B), fitting with the deficiency of BDNF/TrkB signaling in AD. Together, out study provides an innovative mechanism of how BDNF/TrkB neurotrophic signaling mediates APP

metabolism and amyloid pathologies in AD pathologies. In addition to promoting neuronal survival and synaptic plasticity as a neurotrophic factor, BDNF/TrkB pathway directly associates with APP and phosphorylate Y687 residue on its ICD, which regulates its intracellular trafficking and distribution and protects APP from amyloidogenic cleavage by δ-secretase and BACE1, suppressing AD pathogenesis. Clearly, targeting BDNF/TrkB pathway, which is crippled in AD, via small receptor agonists will provide a disease-modifying pharmacologic intervention approach for treating AD.

Acknowledgements This work was supported by grants from NIH grant (RF1, AG051538) to KY, and the National Natural Science Foundation (NSFC) of China (No. 31771114) to XCW. We thank ADRC at Emory University for human AD patients and healthy control samples. This study was supported by the Viral Vector Core of the Emory Neuroscience NINDS Core Facilities (P30NS055077). Additional support by the Rodent Behavioral Core (RBC), which is subsidized by the Emory University School of Medicine and is one of the Emory Integrated Core Facilities. Further support was provided by the Georgia Clinical & Translational Science Alliance of the National Institutes of Health under Award Number UL1TR002378.

Author contributions KY conceived the project, designed the experiments, analyzed the data and wrote the manuscript. YX, ZHW, PL designed and performed most of the experiments. XL prepared primary neurons and bred the animal models. LEM contributed LE-28. LEM and XCW assisted with data analysis and interpretation and critically read the manuscript.

Compliance with ethical standards

Conflict of interest The authors declare that they have no conflict of interest.

Publisher's note Springer Nature remains neutral with regard to jurisdictional claims in published maps and institutional affiliations.

References

1. Reichardt LF. Neurotrophin-regulated signalling pathways. Philos Trans R Soc Lond B Biol Sci. 2006;361:1545–64.
2. Hardy J, Selkoe DJ. The amyloid hypothesis of Alzheimer's disease: progress and problems on the road to therapeutics. Science. 2002;297:353–6.
3. Elliott E, Ginzburg I. The role of neurotrophins and insulin on tau pathology in Alzheimer's disease. Rev Neurosci. 2006;17:635–42.
4. Svendsen CN, Cooper JD, Sofroniew MV. Trophic factor effects on septal cholinergic neurons. Ann NY Acad Sci. 1991;640:91–94.
5. Crutcher KA, Scott SA, Liang S, Everson WV, Weingartner J. Detection of NGF-like activity in human brain tissue: increased levels in Alzheimer's disease. J Neurosci. 1993;13:2540–50.
6. Hellweg R, Gericke CA, Jendroska K, Hartung HD, Cervos-Navarro J. NGF content in the cerebral cortex of non-demented patients with amyloid-plaques and in symptomatic Alzheimer's disease. Int J Dev Neurosci. 1998;16:787–94.
7. Peng S, Wuu J, Mufson EJ, Fahnestock M. Increased proNGF levels in subjects with mild cognitive impairment and mild Alzheimer disease. J Neuropathol Exp Neurol. 2004;63:641–9.
8. Phillips HS, Hains JM, Armanini M, Laramee GR, Johnson SA, Winslow JW. BDNF mRNA is decreased in the hippocampus of individuals with Alzheimer's disease. Neuron. 1991;7:695–702.
9. Connor B, Young D, Yan Q, Faull RL, Synek B, Dragunow M. Brain-derived neurotrophic factor is reduced in Alzheimer's disease. Brain Res Mol Brain Res. 1997;49:71–81.
10. Ferrer I, Marin C, Rey MJ, Ribalta T, Goutan E, Blanco R, et al. BDNF and full-length and truncated TrkB expression in Alzheimer disease. Implications in therapeutic strategies. J Neuropathol Exp Neurol. 1999;58:729–39.
11. Rohe M, Synowitz M, Glass R, Paul SM, Nykjaer A, Willnow TE. Brain-derived neurotrophic factor reduces amyloidogenic processing through control of SORLA gene expression. J Neurosci. 2009;29:15472–8.
12. Matrone C, Ciotti MT, Mercanti D, Marolda R, Calissano PNGF. and BDNF signaling control amyloidogenic route and Abeta production in hippocampal neurons. Proc Natl Acad Sci USA. 2008;105:13139–44.
13. Murer MG, Boissiere F, Yan Q, Hunot S, Villares J, Faucheux B, et al. An immunohistochemical study of the distribution of brain-derived neurotrophic factor in the adult human brain, with particular reference to Alzheimer's disease. Neuroscience. 1999;88:1015–32.
14. Ando S, Kobayashi S, Waki H, Kon K, Fukui F, Tadenuma T, et al. Animal model of dementia induced by entorhinal synaptic damage and partial restoration of cognitive deficits by BDNF and carnitine. J Neurosci Res. 2002;70:519–27.
15. Kitiyanant N, Kitiyanant Y, Svendsen CN, Thangnipon W. BDNF-, IGF-1- and GDNF-secreting human neural progenitor cells rescue amyloid beta-induced toxicity in cultured rat septal neurons. Neurochem Res. 2012;37:143–52.
16. Arancibia S, Silhol M, Mouliere F, Meffre J, Hollinger I, Maurice T, et al. Protective effect of BDNF against beta-amyloid induced neurotoxicity in vitro and in vivo in rats. Neurobiol Dis. 2008;31:316–26.
17. Wang ZH, Xiang J, Liu X, Yu SP, Manfredsson FP, Sandoval IM, et al. Deficiency in BDNF/TrkB Neurotrophic Activity Stimulates delta-Secretase by Upregulating C/EBPbeta in Alzheimer's Disease. Cell Rep. 2019;28:655–669. e655.
18. Wang ZH, Gong K, Liu X, Zhang Z, Sun X, Wei ZZ, et al. C/EBPbeta regulates delta-secretase expression and mediates pathogenesis in mouse models of Alzheimer's disease. Nat Commun. 2018;9:1784.
19. Xiang J, Wang ZH, Ahn EH, Liu X, Yu SP, Manfredsson FP, et al. Delta-secretase-cleaved Tau antagonizes TrkB neurotrophic signalings, mediating Alzheimer's disease pathologies. Proc Natl Acad Sci USA. 2019;116:9094–102.
20. Chen C, Wang Z, Zhang Z, Liu X, Kang SS, Zhang Y, et al. The prodrug of 7,8-dihydroxyflavone development and therapeutic efficacy for treating Alzheimer's disease. Proc Natl Acad Sci USA. 2018;115:578–83.
21. Zhang Z, Liu X, Schroeder JP, Chan CB, Song M, Yu SP, et al. 7,8-dihydroxyflavone prevents synaptic loss and memory deficits in a mouse model of Alzheimer's disease. Neuropsychopharmacology. 2014;39:638–50.
22. Jang SW, Liu X, Yepes M, Shepherd KR, Miller GW, Liu Y, et al. A selective TrkB agonist with potent neurotrophic activities by 7,8-dihydroxyflavone. Proc Natl Acad Sci USA. 2010;107:2687–92.
23. Liu Z, Jang SW, Liu X, Cheng D, Peng J, Yepes M, et al. Neuroprotective actions of PIKE-L by inhibition of SET proteolytic degradation by asparagine endopeptidase. Mol Cell. 2008;29:665–78.
24. Zhang Z, Song M, Liu X, Su Kang S, Duong DM, Seyfried NT, et al. Delta-secretase cleaves amyloid precursor protein and regulates the pathogenesis in Alzheimer's disease. Nat Commun. 2015;6:8762.

25. Zhang Z, Song M, Liu X, Kang SS, Kwon IS, Duong DM, et al. Cleavage of tau by asparagine endopeptidase mediates the neurofibrillary pathology in Alzheimer's disease. Nat Med. 2014;20:1254–62.
26. Bao J, Qin M, Mahaman YAR, Zhang B, Huang F, Zeng K et al. BACE1 SUMOylation increases its stability and escalates the protease activity in Alzheimer's disease. Proc Natl Acad Sci USA. 2018;115:3954–9.
27. Matrone C, Barbagallo AP, La Rosa LR, Florenzano F, Ciotti MT, Mercanti D, et al. APP is phosphorylated by TrkA and regulates NGF/TrkA signaling. J Neurosci. 2011;31:11756–61.
28. Canu N, Amadoro G, Triaca V, Latina V, Sposato V, Corsetti V et al. The intersection of NGF/TrkA signaling and amyloid precursor protein processing in Alzheimer's disease neuropathology. Int J Mol Sci. 2017;18:1319–35.
29. Zhang Z, Kang SS, Liu X, Ahn EH, Zhang Z, He L, et al. Asparagine endopeptidase cleaves alpha-synuclein and mediates pathologic activities in Parkinson's disease. Nat Struct Mol Biol. 2017;24:632–42.
30. Wang ZH, Liu P, Liu X, Manfredsson FP, Sandoval IM, Yu SP, et al. Delta-secretase phosphorylation by SRPK2 enhances its enzymatic activity, provoking pathogenesis in Alzheimer's disease. Mol cell. 2017;67:812–825 e815.
31. Edgington LE, Verdoes M, Ortega A, Withana NP, Lee J, Syed S, et al. Functional imaging of legumain in cancer using a new quenched activity-based probe. J Am Chem Soc. 2013;135:174–82.
32. Li DN, Matthews SP, Antoniou AN, Mazzeo D, Watts C. Multistep autoactivation of asparaginyl endopeptidase in vitro and in vivo. J Biol Chem. 2003;278:38980–90.
33. Zhang Z, Obianyo O, Dall E, Du Y, Fu H, Liu X, et al. Inhibition of delta-secretase improves cognitive functions in mouse models of Alzheimer's disease. Nat Commun. 2017;8:14740.
34. Lunde NN, Haugen MH, Bodin Larsen KB, Damgaard I, Pettersen SJ, Kasem R, et al. Glycosylation is important for legumain localization and processing to active forms but not for cystatin E/M inhibitory functions. Biochimie. 2017;139:27–37.
35. Lee MS, Kao SC, Lemere CA, Xia W, Tseng HC, Zhou Y, et al. APP processing is regulated by cytoplasmic phosphorylation. J Cell Biol. 2003;163:83–95.
36. Scheinfeld MH, Ghersi E, Davies P, D'Adamio L. Amyloid beta protein precursor is phosphorylated by JNK-1 independent of, yet facilitated by, JNK-interacting protein (JIP)-1. J Biol Chem. 2003;278:42058–63.
37. Barbagallo AP, Wang Z, Zheng H, D'Adamio L. A single tyrosine residue in the amyloid precursor protein intracellular domain is essential for developmental function. J Biol Chem. 2011;286:8717–21.
38. Barbagallo AP, Weldon R, Tamayev R, Zhou D, Giliberto L, Foreman O, et al. Tyr(682) in the intracellular domain of APP regulates amyloidogenic APP processing in vivo. PLoS ONE. 2010;5:e15503.
39. Russo C, Dolcini V, Salis S, Venezia V, Violani E, Carlo P, et al. Signal transduction through tyrosine-phosphorylated carboxy-terminal fragments of APP via an enhanced interaction with Shc/Grb2 adaptor proteins in reactive astrocytes of Alzheimer's disease brain. Ann NY Acad Sci. 2002;973:323–33.
40. Tamayev R, Zhou D, D'Adamio L. The interactome of the amyloid beta precursor protein family members is shaped by phosphorylation of their intracellular domains. Mol Neurodegener. 2009;4:28.
41. Tarr PE, Roncarati R, Pelicci G, Pelicci PG, D'Adamio L. Tyrosine phosphorylation of the beta-amyloid precursor protein cytoplasmic tail promotes interaction with Shc. J Biol Chem. 2002;277:16798–804.
42. Alonso M, Medina JH, Pozzo-Miller L. ERK1/2 activation is necessary for BDNF to increase dendritic spine density in hippocampal CA1 pyramidal neurons. Learn Mem. 2004;11:172–8.
43. Amaral MD, Pozzo-Miller L. TRPC3 channels are necessary for brain-derived neurotrophic factor to activate a nonselective cationic current and to induce dendritic spine formation. J Neurosci. 2007;27:5179–89.
44. Rex CS, Lin CY, Kramar EA, Chen LY, Gall CM, Lynch G. Brain-derived neurotrophic factor promotes long-term potentiation-related cytoskeletal changes in adult hippocampus. J Neurosci. 2007;27:3017–29.
45. Triaca V, Sposato V, Bolasco G, Ciotti MT, Pelicci P, Bruni AC, et al. NGF controls APP cleavage by downregulating APP phosphorylation at Thr668: relevance for Alzheimer's disease. Aging Cell. 2016;15:661–72.
46. Rebelo S, Vieira SI, Esselmann H, Wiltfang J, da Cruz e Silva EF, da Cruz e Silva OA. Tyr687 dependent APP endocytosis and Abeta production. J Mol Neurosci. 2007;32:1–8.
47. Rebelo S, Vieira SI, Esselmann H, Wiltfang J, da Cruz e Silva EF, da Cruz e Silva OA. Tyrosine 687 phosphorylated Alzheimer's amyloid precursor protein is retained intracellularly and exhibits a decreased turnover rate. Neurodegener Dis. 2007;4:78–87.
48. Manucat-Tan NB, Saadipour K, Wang YJ, Bobrovskaya L, Zhou XF. Cellular trafficking of amyloid precursor protein in amyloidogenesis physiological and pathological significance. Mol Neurobiol. 2019;56:812–30.